JCTC Journal of Chemical Theory and Computation

Article

pubs.acs.org/JCTC

Diabatic Population Matrix Formalism for Performing Molecular Mechanics Style Simulations with Multiple Electronic States

Jae Woo Park and Young Min Rhee*

Center for Self-Assembly and Complexity, Institute for Basic Science (IBS), Pohang 790-784, Korea

Department of Chemistry, Pohang University of Science and Technology (POSTECH), Pohang 790-784, Korea

Supporting Information

ABSTRACT: An accurate description of nonbonded interactions is important in investigating dynamics of molecular systems. In many situations, fixed point charge models are successfully applied to explaining various chemical phenomena. However, these models with conventional formulations will not be appropriate in elucidating the detailed dynamics during nonadiabatic events. This is mainly because the chemical properties of any molecule, especially its electronic populations, significantly change with respect to molecular distortions in the vicinity of the surface crossing. To overcome this issue in molecular simulations yet within the framework of the fixed point charge model, we define a diabatic electronic population matrix and substitute it for the conventional adiabatic partial charges. We show that this matrix can be readily utilized toward attaining more reliable descriptions of Coulombic interactions, in combination with the interpolation formalism for obtaining the intramolecular interaction potential. We demonstrate how the mixed formalism with the diabatic charges and the interpolation can be applied to molecular simulations by conducting adiabatic and nonadiabatic molecular dynamics trajectory calculations of the green fluorescent protein chromophore anion in aqueous environment.

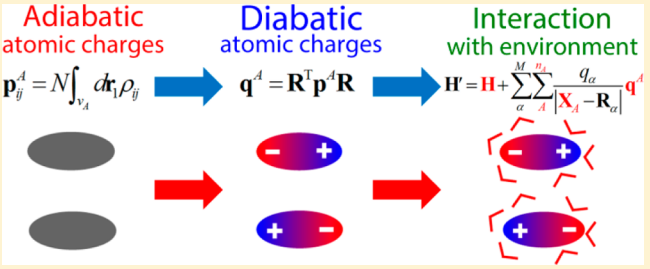

1. INTRODUCTION

Molecular dynamics (MD) is now widely applied to simulating chemical and biological phenomena in various settings.[1,2] In recent years, its utility has expanded to investigating systems with electronic excitations. In elucidating the dynamics of excited molecules, especially in the condensed phase, methods that incorporate direct quantum chemical calculations are often adopted without explicitly constructing their potential energy surfaces (PESs).[3,4] This is in part to avoid the complications associated with generating potential energy surfaces of the involved excited states in any functional forms. However, obtaining excited state potential information with quantum chemical means is highly time-consuming in general, and the applicability of MD with direct quantum chemical calculations is limited either in its simulation time or in its level of reliability. To overcome this computational cost issue, the interpolated mechanics/molecular mechanics (IM/MM) has been recently suggested as a more economic approach, with an explicit construction of the PES for the system of interest.[5] This method adopts an interpolated PES[6−23] to describe the internal motion of the important part in the system. This technique has been successfully applied for conducting simulations of an electronically excited protein with a statistically meaningful number of trajectories for relatively long durations.[5] It was also shown that nonadiabatic phenomena can be described by implementing the quasi-diabatic potential energy matrix interpolation scheme.[22−25]

In IM/MM, nonbonded interactions for dispersion and electrostatics are described by the conventional molecular mechanics approach with parametrized factors.[5] For electrostatic interactions, the fixed point charge model based on restrained electrostatic potential fitted charges[26] or natural atomic charges[27] will be the simplest and likely the most widely applied scheme. Even the more advanced polarizable models[28−48] rely on fixed point charges in various places in their formulations. Conventionally, the fixed charges are fitted at the most stable conformation (commonly called equilibrium geometry). For simulations with multiple electronic states, this will correspond to minimum energy configurations on different adiabatic electronic states. In our first attempt of IM/MM in nonadiabatic simulations, we have indeed performed parametrizations through such processes.[5,8,49,50] However, this approach will be reliable only when the atomic motion is small and limited around the minimum energy configuration without encountering any surface crossing.[1,2,8,50] In the case of nonadiabatic dynamics, electrostatic properties of the adiabatic states will change to large extents especially around surface crossing points.[51−58] This will subsequently alter the nonbonded interactions between the molecule and its surrounding. In addition, because the degree of such alterations will be different for different electronic states, the surface crossing points will inevitably migrate in comparison to the gas phase

Received: July 31, 2014

   dx.doi.org/10.1021/ct5006856 | J. Chem. Theory Comput. XXXX, XXX, XXX−XXX

situation. This will further modify the dynamics of the system in a complex manner. Simply, because the gap energy and the locations of the crossing points between different electronic states importantly contribute to the characteristics of interstate crossing,[4,24,59] accurately describing solute−solvent or chromophore−protein electrostatic interactions will be essential for performing reliable nonadiabatic dynamics simulations.

This aspect leads us to imagine that adopting diabatic point charges, instead of adiabatic ones, will be physically more appropriate. This can be predicted from the fact that the diabatic states normally are much less susceptible to molecular deformations.[60] Because the diabatic-to-adiabatic transform relation will likely be geometry dependent, the fixed diabatic point charge model will lead to adiabatic point charges that change with different molecular geometries. Utilizing these charges will yield a much improved description of solute−solvent interactions as depicted in Figure 1. In this simple example, we imagine a situation with a solvated system with two diabatic electronic states that cross at a certain geometry (Figure 1a). When the fixed adiabatic charge model is used, the atomic charge distributions on the molecule will be the same at all geometries, and therefore, a stabilization effect due to the solvation will be similar along the "reaction coordinate" A → B (Figure 1b). However, in a real situation, the electrostatic characteristics of the adiabatic surface indeed will change around the surface crossing point. Therefore, the solvation energy will subsequently change even when the solvent structure is not changed along the reaction coordinate (Figure 1c). This change in the effective potential surface will further alter the solvation dynamics along the reaction coordinate. More importantly, the surface crossing point will be displaced through the solvation as depicted in the figure. Because simulations with fixed *adiabatic* partial charges will not be capable of handling these features, employing fixed *diabatic* charges will indeed be more preferable toward obtaining at least qualitatively correct descriptions of solvation and the related surface crossing dynamics.

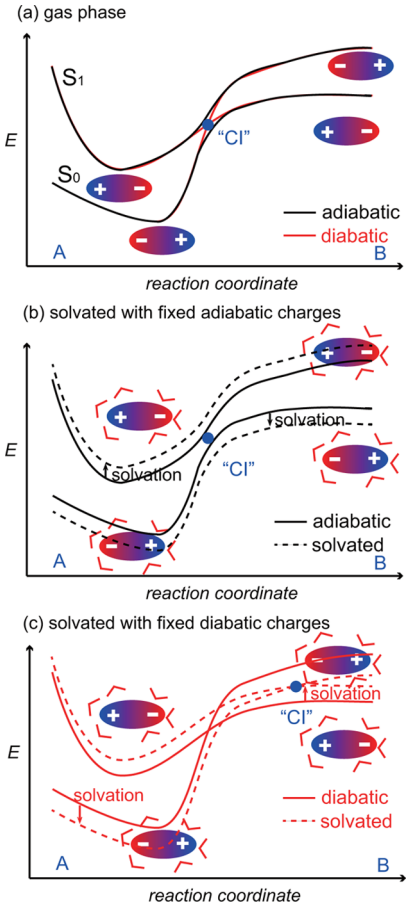

Figure 1. Schematic diagram that compares the modeling schemes of a chromophore system with two electronic states (a) in the gas phase, (b) in solution with fixed adiabatic charges, and (c) in solution with fixed diabatic charges. The fixed adiabatic charges of the two states will be fitted at the geometries A (S_0) and B (S_1). With the fixed adiabatic charges, the solvation energy will be similar when the solvation shell structure is the same. On the contrary, with the diabatic charges, the Coulomb interaction between the solute and the solvent will be different with different molecular geometries. In addition, the conical intersection will displace due to different solvation energies of the two diabatic states as shown in (c). Of course, the diabatic representation will be closer to the real physics.

One obvious example molecule of this type will be the green fluorescent protein (GFP) chromophore, *para*-hydroxybenzylidene imidazolinone (*p*HBI), shown in Figure 2. This

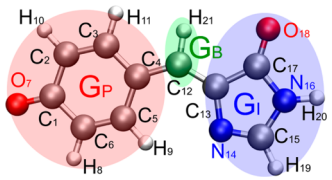

Figure 2. *p*HBI anion structure with the atom and the group designations adopted in this work.

fluorophore has two intramolecular twisting pathways toward surface crossing points, which are often termed as the imidazolinone channel and the phenoxy channel.[53,54,61] The charge localization behaviors in this molecule differ by the channels. Specifically, when *p*HBI twists in the first excited state along the imidazolinone channel, the electron density is shifted toward the phenoxy ring. On the other hand, when it twists along the phenoxy channel, the negative charge is shifted toward the imidazolinone ring. Using adiabatic partial charges indeed cannot describe this phenomenon and the electrons are distributed almost evenly on the two rings when the chromophore geometry is planar.[53] Because a three-state quasi-diabatic representation of the chromophore describes the charge transfer on adiabatic surfaces quite well,[53] a proper modeling of the electrostatic interactions should become possible by adopting this quasi-diabatization scheme. Such a scheme will lead to more reliable excited state dynamics simulations of GFP and other related species at a reasonable computational cost when it is coupled with economic simulation tactics such as interpolation.

In this article, we present such a scheme for generating diabatic fixed charges toward improved description of electrostatic interactions in nonadiabatic IM/MM simulations. Based on an assumption that the characteristics of diabatic states remain rather invariant with respect to molecular distortions,[60] which we indeed see at least for *p*HBI, we obtain fixed diabatic atomic charge distributions by defining diabatic electronic population matrices. With the diabatic electronic population matrix of the chromophore, we compute the electrostatic interaction energies with the environment for all diabatic states and convert these into adiabatic energies through diagonaliza-

dx.doi.org/10.1021/ct5006856 | J. Chem. Theory Comput. XXXX, XXX, XXX−XXX

tion. This approach of course can be performed in an on-the-fly manner during trajectory simulations. We demonstrate the utility of the fixed diabatic charge model by applying it to the nonradiative decay simulations of the *p*HBI molecule. We present additional advantages of adopting our diabatic charge formalism for MD simulations, together with discussions on its limitations. Potential future improvements toward lifting the limitations are also discussed as concluding remarks of the present work.

2. THEORY AND SIMULATION METHODS

In this section, we will first briefly overview the methods for determining diabatic states and for interpolating the diabatic potential energy matrices, with a specific example of the green fluorescent protein chromophore. Through these methods, we can obtain not only adiabatic energies and nonadiabatic couplings but also the adiabatic-to-diabatic transformation matrix at any arbitrary molecular geometry. The adiabatic-to-diabatic transformation indeed dictates how the diabatic states can remix to form different adiabatic states. We will then define a Hamiltonian for describing the interactions between the chromophore and its surrounding charges and will show how this Hamiltonian can be approximated for imposing the condition for the rather simple point charge model. With this, we will derive the diabatic electronic population matrix formalism and then subsequently define atomic partial charges and other physical quantities required for obtaining the matrix. We will also describe how these quantities can be obtained within quantum chemical approaches, with a specific example of the multiconfiguration self-consistent field (MCSCF) theory. The detailed procedures of demonstrational simulations will also be presented.

Determining Diabatic States. Quantum chemical calculations normally yield adiabatic state information. The wave functions of such adiabatic states are transformed with the adiabatic-to-diabatic transformation matrix **R** as

$$\Psi_a^{\mathrm{dia}} = \sum_b R_{ba} \Psi_b^{\mathrm{adia}} \tag{1}$$

Here, Ψ_a^{dia} and Ψ_b^{adia} are the wave functions of the *a*-th diabatic and the *b*-th adiabatic states, respectively.[22−25,53,62] There have been many reports on practical ways for determining diabatic states.[62−89] In approaches based on the valence bond (VB) theory, the diabatic states are often first constructed based on chemical intuitions and then their corresponding adiabatic states are obtained from their mixtures.[73−76] Similar in spirit to these valence bond approaches, the constrained density functional theory can be used to construct diabatic states by forcing electronic densities to conform to similar chemical intuitions.[70,71] In contrast, there are methods that construct the adiabatic wave functions first and then extract the VB type information for diabatization. For example, in the block-localized wave function (BLW) approach,[79−82] the electrons and their primitive basis set functions in a given system are first partitioned into subgroups, and BLWs for defining diabatic states are constructed as antisymmetrized products of molecular orbitals by linearly combining the subgroup basis functions.[80] In the molecular orbital valence bond (MOVB) method,[76−78] as an extension of the BLW approach, the VB type configuration interaction Hamiltonian is constructed with diabatic wave functions defined with BLWs. From a conceptual point of view, diabatic transformations that remove derivative coupling elements can also be designed. In reality, however, completely eliminating derivative coupling vectors is not possible for polyatomic molecules with more than three atoms.[69] Therefore, in practice, quasi-diabatizations with negligible but still nonvanishing amounts of residual couplings are normally adopted in direct transformations.[67,68] Because computing nonadiabatic coupling matrix elements is often very expensive, the transform is often based on physical or mathematical intuitions rather than the coupling itself. For example, in the block diagonalization algorithm,[62−65] diabatic states are constructed from projections of adiabatic states onto a specific model diabatic space. Methods that enforce consistencies of dominant configurations or uniformities of physical observables are also available for generating diabatic PESs.[83−88]

In this work, we employ the unitary block diagonalization formalism developed by Pacher et al.[62] For this, three diabatic states for GFP chromophore are defined with the Foster-Boys localized orbitals named as *p*, *b*, and *i* as shown in Figure 3.[90]

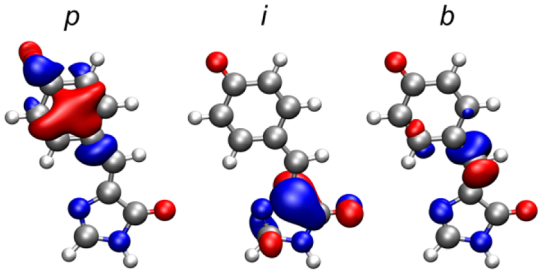

Figure 3. Three localized orbitals generated by the Foster−Boys localization scheme within the active space.

The localization is conducted within the space of active orbitals, which are optimized using the three-state averaged, four electrons in three orbitals complete active space self-consistent field (SA-CAS(4,3)) theory. These localized orbital are of course mutually orthogonal to each other. The three diabatic states are denoted as P-state, I-state, and B-state, and their dominant parts are covalent determinants $|ppbi\rangle$, $|iipb\rangle$, and $|bbpi\rangle$, respectively. In fact, the same localization-based diabatization scheme has been applied to other symmetric monomethine dyes.[91,92] For more details, see the previous report by Olsen et al.[53]

Interpolating Gas Phase Diabatic Hamiltonian. Even though our diabatic electronic population formalism can be compatible with many different formulations of the intramolecular potential of the chromophore, we will mainly focus on the interpolation scheme as a way of forming the total potential. This is because the aim for constructing a new diabatic property is to apply it to studying nonadiabatic behaviors, where the intramolecular potential over a large space of molecular conformations is needed, and because the interpolation performs much more reliably than conventional molecular force fields for this purpose.

From the definition of the adiabatic-to-diabatic transformation matrix (eq 1), we can obtain the diabatic Hamiltonian **D** with the adiabatic potential energy matrix **V** at a data point geometry $\mathbf{X}(n)$ as

$$\mathbf{D}(\mathbf{X}(n)) = \mathbf{R}^{\mathrm{T}}(\mathbf{X}(n))\mathbf{V}(\mathbf{X}(n))\mathbf{R}(\mathbf{X}(n)) \tag{2}$$

Interpolated **D** at an arbitrary geometry **X** is computed by a weighted average over PES information from *N* data points as described by Collins and co-workers:[23]

dx.doi.org/10.1021/ct5006856 | J. Chem. Theory Comput. XXXX, XXX, XXX−XXX

$$\mathbf{D}(\mathbf{X}) = \sum_{n}^{N} w(\mathbf{X};\, \mathbf{X}(n))\mathbf{D}(\mathbf{X};\, \mathbf{X}(n)) \tag{3}$$

Here, $\mathbf{D}(\mathbf{X};\mathbf{X}(n))$ is the Taylor-expanded diabatic Hamiltonian from a data point geometry $\mathbf{X}(n)$, and $w(\mathbf{X};\mathbf{X}(n))$ is an interpolating weighting function. The internal coordinates were utilized for taking the first and second derivatives of the diabatic Hamiltonian in this work together with Cartesian coordinates for weighting,[7] among a number of different options available.[17−20,23] Because computing the second derivatives of the adiabatic energies is very costly, one can employ the dual-level interpolation approach.[6,93] The derivatives of interpolated diabatic potential energy matrix are given by[22−24,93]

$$\frac{\partial \mathbf{D}(\mathbf{X})}{\partial X_a} = \sum_{n}^{N} w(\mathbf{X};\, \mathbf{X}(n))\frac{\partial \mathbf{D}(\mathbf{X};\, \mathbf{X}(n))}{\partial X_a} + \mathbf{D}(\mathbf{X};\, \mathbf{X}(n)) \times \sum_{n}^{N} \frac{\partial w(\mathbf{X};\, \mathbf{X}(n))}{\partial X_a} \tag{4}$$

With this interpolated diabatic Hamiltonian matrix, we can obtain the adiabatic state information by diagonalizing the matrix $\mathbf{D}(\mathbf{X})$ after interpolation:

$$\mathbf{V} = \mathbf{R}\mathbf{D}\mathbf{R}^{\mathrm{T}} \tag{5}$$

We can also calculate the derivative coupling vectors between two adiabatic states k and j as

$$(\mathbf{F}_{jk})_a = -\frac{\mathbf{e}_j^{\mathrm{T}}(\partial \mathbf{D}/\partial X_a)\mathbf{e}_k}{V_{jj} - V_{kk}} \tag{6}$$

where $\mathbf{e}_i$ is the i-th eigenvector of $\mathbf{D}$, namely the i-th row vector of $\mathbf{R}$. Of course, its elements constitute the transformation rule from the diabatic states into the i-th adiabatic state.[24]

Diabatic Electronic Population Matrix. Now, let us consider the case of inserting the chromophore molecule into a bath of external charges. The diabatic Hamiltonian in the gas phase,

$$D_{ab} = \langle \Psi_a^{\mathrm{dia}} | H_0 | \Psi_b^{\mathrm{dia}} \rangle \tag{7}$$

will be perturbed by the interactions between the molecule and the external charges as

$$D'_{ab} = \langle \Psi_a^{\mathrm{dia}} | H_0 + H_{\mathrm{c}} | \Psi_b^{\mathrm{dia}} \rangle = \langle \Psi_a^{\mathrm{dia}} | H_0 | \Psi_b^{\mathrm{dia}} \rangle + \langle \Psi_a^{\mathrm{dia}} | H_{\mathrm{c}} | \Psi_b^{\mathrm{dia}} \rangle \tag{8}$$

Here, of course, H_{c} defines the interaction term that couples the chromophore and the bath (namely, the external MM charges). We also assume that the form of H_0 is not affected by the coupling interaction. Then, the first integral term with H_0 is identical to the formulation in the gas phase and is readily obtained with the interpolation described in the previous part. The interaction Hamiltonian term can be written as

$$H_{\mathrm{c}} = \sum_{i}^{N}\sum_{\alpha}^{M} \frac{q_\alpha}{r_{i\alpha}} \tag{9}$$

where q_α is the charge of the α-th bath particle, whose distance from the i-th electron is $r_{i\alpha} = |\mathbf{r}_i - \mathbf{R}_\alpha|$. Of course, N and M are the numbers of the electrons and the bath particles in the system. Therefore, the last term in eq 8 can be written as

$$\langle \Psi_a^{\mathrm{dia}} | H_{\mathrm{c}} | \Psi_b^{\mathrm{dia}} \rangle = N \sum_{\alpha}^{M} \int d\mathbf{r}_1 d\mathbf{r}_2 \ldots d\mathbf{r}_N \Psi_a^{\mathrm{dia}*}(\mathbf{r}_1, \mathbf{r}_2, \ldots, \mathbf{r}_N) \times \frac{q_\alpha}{r_{1\alpha}} \Psi_b^{\mathrm{dia}}(\mathbf{r}_1, \mathbf{r}_2, \ldots, \mathbf{r}_N) \tag{10}$$

To simplify this expression, we define a one-particle density matrix element (diagonal) and one-particle transition density matrix element (off-diagonal)[94] between states a and b:

$$\rho_{ab}(\mathbf{r}_1) \equiv N \int d\mathbf{r}_2 d\mathbf{r}_3 \cdots d\mathbf{r}_N \Psi_a^{\mathrm{dia}}(\mathbf{r}_1, \mathbf{r}_2, \cdots, \mathbf{r}_N)\Psi_b^{\mathrm{dia}*}(\mathbf{r}_1, \mathbf{r}_2, \cdots, \mathbf{r}_N) \tag{11}$$

Physically, the off-diagonal elements measure the one-electron character in the transition between the two involved electronic states.[94] In any case, with this density matrix, the coupling interaction term becomes

$$\langle \Psi_a^{\mathrm{dia}} | H_{\mathrm{c}} | \Psi_b^{\mathrm{dia}} \rangle = \sum_{\alpha}^{M} \int d\mathbf{r}_1 \rho_{ba}(\mathbf{r}_1) \frac{q_\alpha}{r_{1\alpha}} \tag{12}$$

To impose the atomic point charge approximation on this expression, we additionally define an electronic population matrix on an atom A by integrating the one-particle density in the space ν_{A} spanned by the atom A, namely $\mathbf{q}_{ab}^{\mathrm{A}} \equiv \int_{\nu_{\mathrm{A}}} d\mathbf{r}\rho_{ab}(\mathbf{r})$.[95] With the point charge approximation, we assume that the electron distribution on the atom A is represented as a charge at the position of the nucleus $\mathbf{X}_{\mathrm{A}}$. Then, when there are n_{A} atoms in the chromophore, the coupling electrostatic interaction energy becomes

$$\langle \Psi_a^{\mathrm{dia}} | H_{\mathrm{c}} | \Psi_b^{\mathrm{dia}} \rangle = \sum_{\alpha}^{M}\sum_{\mathrm{A}}^{n_{\mathrm{A}}} \int_{\nu_{\mathrm{A}}} d\mathbf{r}_1 \rho_{ba}(\mathbf{r}_1) \frac{q_\alpha}{r_{1\alpha}} \approx \sum_{\alpha}^{M}\sum_{\mathrm{A}}^{n_{\mathrm{A}}} \frac{q_\alpha}{|\mathbf{X}_{\mathrm{A}} - \mathbf{R}_\alpha|} \mathbf{q}_{ba}^{\mathrm{A}} \tag{13}$$

With this, the electrostatic interaction contributions in the diabatic basis are evaluated and then added to the gas phase Hamiltonian. Its overall working expression is then

$$\mathbf{D}'(\mathbf{X};\, \mathbf{R}) = \mathbf{D}(\mathbf{X}) + \sum_{\alpha}^{M}\sum_{\mathrm{A}}^{n_{\mathrm{A}}} \frac{q_\alpha}{|\mathbf{X}_{\mathrm{A}} - \mathbf{R}_\alpha|} \mathbf{q}^{\mathrm{A}} \tag{14}$$

To utilize this formulation in the actual molecular simulations, the electron densities on the chromophore atoms are needed, which can normally be supplied by electronic structure calculations. Because quantum chemical calculations primarily yield adiabatic information, the adiabatic electronic population on the atom A is first defined as

$$\mathbf{p}_{ij}^{\mathrm{A}} \equiv N \int_{\nu_{\mathrm{A}}} d\mathbf{r}_1 \int d\mathbf{r}_2 d\mathbf{r}_3 \cdots d\mathbf{r}_N \Psi_i^{\mathrm{adia}}(\mathbf{r}_1, \mathbf{r}_2, \cdots, \mathbf{r}_N)\Psi_j^{\mathrm{adia}*}(\mathbf{r}_1, \mathbf{r}_2, \cdots, \mathbf{r}_N) \tag{15}$$

and is transformed into the diabatic electronic population as

$$\mathbf{q}^{\mathrm{A}} = \mathbf{R}^{\mathrm{T}}\mathbf{p}^{\mathrm{A}}\mathbf{R} \tag{16}$$

Of course, this transformation is trace-conserving with its back-transform well-defined on the condition that $\mathbf{R}$ is well-defined.

Determining Electronic Population Matrix. Before discussing the formalism for obtaining the electronic population

dx.doi.org/10.1021/ct5006856 | J. Chem. Theory Comput. XXXX, XXX, XXX−XXX

matrix, let us first consider how the atomic spans can be defined. For this purpose, we employ the natural population analysis based formalism, which yields straightforward definitions of the electronic population matrix and the atomic spaces.[27] We note that utilizing any types of charges, including the electrostatic potential fitted atomic partial charges[96] in the adiabatic electronic population matrix should also be possible in principle with appropriate definitions of transition density matrix elements and their atomic separations. Here, however, we will resort to the natural population analysis as a means to attain atomization and demonstrate how the electronic population matrices are defined within MCSCF theory. The electronic population matrices with multiple electronic states can be similarly defined within any quantum chemical formalisms with Slater determinant expansions, such as the methods based on configuration interaction singles (CIS)[97−100] or their perturbative corrections.[99−103]

In MCSCF, the wave function Ψ of an arbitrary state is written as a weighted sum over a set of Slater determinants or electronic configurations ψ_I. Then the one-particle densities in eq 11 involving $\Psi_i = \sum_I c_I^i \psi_I$ and $\Psi_j = \sum_J c_J^j \psi_J$ is related to its matrix counterpart:[95]

$$\gamma_{ij}(\mathbf{r}_1, \mathbf{r}_1') = N \sum_{IJ} c_I^i c_J^{j*} \int d\mathbf{r}_2 d\mathbf{r}_3 \cdots d\mathbf{r}_N \psi_I(\mathbf{r}_1, \mathbf{r}_2, \cdots, \mathbf{r}_N) \times \psi_J^*(\mathbf{r}_1', \mathbf{r}_2, \cdots, \mathbf{r}_N) \tag{17}$$

When this density is integrated in an infinitely large space, the result will simply be

$$\int d\mathbf{r}_1 \gamma_{ij}(\mathbf{r}_1, \mathbf{r}_1) \equiv \int d\mathbf{r}_1 \rho_{ij}(\mathbf{r}_1) = N\delta_{ij} \tag{18}$$

However, the off-diagonal integrals with $i \neq j$ do not vanish in the atomic subspace. Indeed, nonvanishing terms are generated from the cases with $\psi_J = \psi_I$ or $\psi_J = a_q^\dagger a_p \psi_I$, where $a_q^\dagger$ and a_p are the creation and the annihilation operators in the language of second quantization.[95,104] Then, it is easy to show that the elements of the electronic population matrix are written with the molecular orbital basis $\{\varphi\}$ as

$$\gamma_{ij}(\mathbf{r}_1, \mathbf{r}_1') = N \sum_I c_I^i \Big(c_I^{j*} \sum_p^{\{p\}_I} \varphi_p(\mathbf{r}_1) \varphi_p^*(\mathbf{r}_1') + \sum_{J\neq I}^{\{I(q,r)\}} c_J^{j*} \sum_{p\neq r}^{\{p\}_I} \varphi_p(\mathbf{r}_1) \varphi_q^*(\mathbf{r}_1') \Big) \tag{19}$$

where $\{p\}_I$ symbolically represents a set with all p values satisfying $a_p\psi_I \neq 0$. In addition, $\{I(q,r)\}$ denotes the set of indices of nonvanishing configurations $a_q^\dagger a_r \psi_I$ with $q \neq r$.

To introduce atomic subspaces for the integration in eq 18, a natural atomic orbital (NAO) based formalism is employed. This process begins with the construction of the electronic population matrix $\mathbf{O}^{\mathrm{MO}}$ in the molecular orbital (MO) basis, whose (p,q)-th element is calculated as

$$[\mathbf{O}_{ij}^{\mathrm{MO}}]_{pq} = \int d\mathbf{r}_1 d\mathbf{r}_1' \varphi_p^*(\mathbf{r}_1) \gamma_{ij}(\mathbf{r}_1, \mathbf{r}_1') \varphi_q(\mathbf{r}_1') \tag{20}$$

When $i = j$, of course, this matrix becomes the conventional one-electron reduced density matrix.[95] The electronic population matrix in the atomic orbital (AO) basis, $\mathbf{O}^{\mathrm{AO}}$, is computed as

$$\mathbf{O}_{ij}^{\mathrm{AO}} = \mathbf{S}\mathbf{C}\mathbf{O}_{ij}^{\mathrm{MO}}\mathbf{C}^{\mathrm{T}}\mathbf{S}^{\mathrm{T}} \tag{21}$$

with the atomic orbital basis overlap matrix $\mathbf{S}$ and the MO coefficients $\mathbf{C}$.[27] We then transform $\mathbf{O}^{\mathrm{AO}}$ into the NAO basis with the matrix $\mathbf{T}$:[27]

$$\mathbf{O}_{ij}^{\mathrm{NAO}} = \mathbf{T}^{\mathrm{T}}\mathbf{O}_{ij}^{\mathrm{AO}}\mathbf{T} \tag{22}$$

Now we can replace the integral over an atomic span (v_A) in eq 15 with the atomic partial sum over natural atomic orbitals to generate the elements of the adiabatic electronic population matrix for individual atoms:

$$\mathbf{p}_{ij}^{\mathrm{A}} = \sum_{\mu}^{(\mathrm{A})} [\mathbf{O}_{ij}^{\mathrm{NAO}}]_{\mu\mu} \tag{23}$$

Here, μ is the index of the natural atomic orbitals and "(A)" symbolically represents the NAO set on the atom A. The nondiagonal elements are not included in the summation, as they vanish due to the orthonormality of natural atomic orbitals.

Molecular Simulation Using Diabatic Partial Charges. From the fact that the chemical properties of the electronic states are well preserved with respect to nuclear displacements with the diabatic states,[60] let us assume that the diabatic electronic population matrix on each atom does not change upon distortions of the molecule. In fact, this is the key assumption of the fixed diabatic partial charge model. Of course, the elements of the diabatic electronic population matrix will vary to some degree at different geometries and this variation will correspond to "internal polarization" in the diabatic states. Even though the interpolation technique should in principle be able to handle this type of polarization by additionally interpolating the partial charges, in the current work, we will stick to the more manageable fixed charge model. In later sections, we will show that this fixed charge approximation is at least qualitatively appropriate in treating the model chromophore.

Within the framework of IM/MM, the interactions between the interpolated chromophore and the environment for all diabatic states are first calculated and added to the diabatic Hamiltonian as shown with eq 14. Because we adopt the fixed point charge model, the diabatic electronic population matrix of the IM area is kept constant during molecular simulations. The perturbed Hamiltonian $\mathbf{D}'$ is calculated at any given geometry and then diagonalized to obtain adiabatic potential energies $\mathbf{V}'$ and the diabatic-to-adiabatic transform matrix $\mathbf{R}'$ as

$$\mathbf{V}' = \mathbf{R}'\mathbf{D}'\mathbf{R}'^{\mathrm{T}} \tag{24}$$

The force in the i-th adiabatic state will be related to the first derivative of the i-th eigenvalue of $\mathbf{D}'$ with respect to an arbitrary Cartesian coordinate X_a. It is trivial to show that the adiabatic gradient computed with $\mathbf{R}'$ and the diabatic derivative is given as[105]

$$\frac{\partial V_i'}{\partial X_a} = \left[\mathbf{R}' \frac{\partial \mathbf{D}'}{\partial X_a} \mathbf{R}'^{\mathrm{T}} \right]_{ii} \tag{25}$$

Of course, the correctness of the gradient implementation can be practically ensured by checking the energy conservations with constant-energy and constant-volume (NVE) style simulations.

Computational Details. We first computed the diabatic electronic population matrices of all the atoms in pHBI with the SA3-CAS(4,3) level of theory with the 6-31G(d) basis set. The effect of adding diffuse basis functions to the PES characteristics

dx.doi.org/10.1021/ct5006856 | J. Chem. Theory Comput. XXXX, XXX, XXX−XXX

Table 1. Diabatic Electronic Populations Computed with Natural Populations[a]

$$\mathbf{q} = \begin{pmatrix} q_{PP} & q_{PI} & q_{PB} \\ q_{PI} & q_{II} & q_{IB} \\ q_{PB} & q_{IB} & q_{BB} \end{pmatrix}$$

moiety	atom/group[b]	q_{PP}	q_{II}	q_{BB}	q_{PI}	q_{PB}	q_{IB}
phenoxy	C_1	0.487	0.609	0.513	−0.024	−0.029	0.009
	C_2	−0.434	−0.311	−0.301	0.029	0.020	0.009
	C_3	−0.182	−0.123	−0.218	−0.028	−0.028	−0.001
	C_4	−0.241	−0.115	−0.023	0.092	0.065	0.004
	C_5	−0.185	−0.131	−0.239	−0.035	−0.031	−0.005
	C_6	−0.443	−0.298	−0.312	0.018	0.011	0.012
	O_7	−0.876	−0.693	−0.743	0.005	−0.003	0.016
	H_8	0.216	0.216	0.216	0.000	0.000	0.000
	H_9	0.238	0.238	0.238	0.000	0.000	0.000
	H_{10}	0.217	0.217	0.217	0.000	0.000	0.000
	H_{11}	0.205	0.205	0.205	0.000	0.000	0.000
	G_P	−0.997	−0.186	−0.446	0.059	0.006	0.044
imidazolinone	C_{13}	0.048	−0.233	0.092	0.084	0.018	0.057
	N_{14}	−0.570	−0.525	−0.565	−0.005	−0.017	0.012
	C_{15}	0.379	0.131	0.260	−0.012	0.022	−0.027
	N_{16}	−0.737	−0.734	−0.732	0.001	−0.001	0.003
	C_{17}	0.827	0.650	0.688	−0.028	0.014	−0.042
	O_{18}	−0.711	−0.874	−0.762	0.006	0.014	−0.006
	H_{19}	0.191	0.191	0.191	0.000	0.000	0.000
	H_{20}	0.422	0.422	0.422	0.000	0.000	0.000
	G_I	−0.153	−0.972	−0.406	0.046	0.051	−0.002
bridge	C_{12}	−0.068	−0.059	−0.365	−0.105	−0.056	−0.042
	H_{21}	0.218	0.218	0.218	0.000	0.000	0.000
	G_B	0.149	0.158	−0.147	−0.105	−0.056	−0.042

[a]The **q** values shown here are the negatives of the diabatic electronic population matrix elements. The diagonal elements also include nuclear charges to better reflect atomic partial charges. [b]Atom and group designations are found in Figure 2.

is known to be only marginal.[53] The charge diabatization was performed at the S_0-optimized geometry, which was also utilized for obtaining dispersive interaction parameters in our previous work.[93] The ansatz that was adopted in that work for the geometry optimization was actually SA2-CAS(4,3)/6-31+G(d). The slight geometric discrepancy from the geometry at the SA3-CAS(4,3)/6-31G(d) level will be insignificant for our fixed charge model. Besides, the interpolation approach is in principle not affected by that discrepancy.

Because we are using the state averaged multireference quantum chemical theory, the atomic orbital to natural atomic orbital transformation matrix **T** will be somewhat state-dependent. Instead of selecting one of the SA3-CAS(4,3) states for defining natural orbitals toward the charge atomizations, we have adopted the Hartree−Fock electron density. With this, after computing atomic electronic populations as shown in eqs 22 and 23, the adiabatic atomic partial charges are transformed to $\mathbf{q}^A$ (eq 16) with **R** from the block-diagonalization quasi-diabatization method.[53,62,64]

To test the applicability of our scheme to describing complex molecular systems, we generated a system with a *p*HBI anion solvated in water. The initial conformation was produced by creating a periodic cubic box with the side length of 40.0 Å and by placing one *p*HBI anion at its center. This was then immersed in water and energy minimized using the steepest descent method.[106] The minimized geometry was equilibrated using an isobaric−isothermal (*NPT*) condition with ambient temperature (300 K) and pressure (1.0 bar), by adopting Berendsen's weak coupling algorithms[107] with a time constant of τ = 2.0 ps for the initial 50 ps and then by using Nosé−Hoover thermostat[108] and Parrinello−Rahman barostat[109] for the next 50 ps. Starting from the equilibrated conformation, an MD trajectory of 1 ns duration was obtained to collect an ensemble of 500 independent solvated structures. These structures were employed in the following calculations.

The accuracies of electrostatic energy evaluations using our diabatic electronic population matrix were then checked against mixed quantum mechanical/molecular mechanical (QM/MM) energies through the following procedures. Test conformations with the *p*HBI anion solvated in water were generated by propagating independent excited state (S_1) trajectories for 3.0 ps durations with the same *NPT* condition, starting from the 500 structures that were mentioned in the above. These trajectories usually reached twisted geometries within 2.0 ps after initiations, which are rather far from the Franck−Condon point. As they cover a large conformational space, adopting them for monitoring the reliability of electrostatic energies will be reasonable. The conformations were recorded at 1.0 ps intervals including the ones at time zero, giving a total of 2000 test samples from the 500 trajectories. The electrostatic energies at these conformations were calculated by IM/MM with the diabatic electronic population matrix and then compared against the electrostatically embedded QM/MM values as references. IM/MM energies with fixed adiabatic charges were also checked for comparison. In all these calculations, water molecules were described with the TIP3P model.[110] The SA3-CAS(4,3) level of theory were used for the QM part in the QM/MM calculations.

dx.doi.org/10.1021/ct5006856 | J. Chem. Theory Comput. XXXX, XXX, XXX−XXX

To additionally demonstrate the applicability of the present scheme, we have also conducted molecular simulations of the solvated *p*HBI anion in the following manner. Nonadiabatic simulations were started from the same 500 solvated structures, by adopting the fewest switches[111,112] and the Landau−Zener type[111,113,114] surface hopping formalisms. In the fewest switches surface hopping algorithm, the quantum amplitude of an adiabatic state k (C_k) is integrated in time with

$$i\hbar\frac{dC_k}{dt} = E_kC_k - i\hbar\sum_j C_j\mathbf{F}_{kj}\cdot\mathbf{v} \tag{26}$$

where E_k, $\mathbf{F}_{kj}$, and $\mathbf{v}$ are the energy of the state k, the derivative coupling vector between the states k and j, and the nuclear velocity, respectively. A uniform random number is generated at each time step $t + \Delta t$, and when the random number is smaller than a quantity g_{kj},

$$g_{kj} = \frac{-2\int_t^{t+\Delta t}\mathrm{Re}(C_k^*C_j)\mathbf{F}_{kj}\cdot\mathbf{v}d\tau}{\mathrm{Re}(C_k^*C_k)} \tag{27}$$

the hop is accepted. As usual, with each hop, the energy is conserved by scaling the velocity component along $\mathbf{F}_{kj}$. When the energy conservation fails, the velocity component is simply reversed.[93,111,112,115] In the Landau−Zener type surface hopping, the probability of a transition between two electronic states k and j is defined by

$$P = \exp\left(-\frac{\pi}{4}\frac{E_k - E_j}{\hbar\mathbf{F}_{kj}\cdot\mathbf{v}}\right) \tag{28}$$

We have adopted hopping conditions following the previous work by Morokuma and co-workers,[4] so that nonadiabatic crossing occurs when P was larger than 0.5 or when $E_k - E_j$ was smaller than 0.6275 kcal/mol. Each nonadiabatic trajectory was integrated up to 2.0 ps. These nonadiabatic MD simulations were conducted with the *NVE* condition without imposing any thermostat or barostat algorithms.

In all IM/MM simulations, previously constructed SA3-CAS(4,3) and SA3-CAS(4,3)-PT2 data sets[24] with 1500 data points were employed toward the interpolation for describing the *p*HBI internal motion and its diabatic mixing. Dispersive energies were taken to be the same in both S_0 and S_1 states, whose parameters were previously obtained in the S_0 state.[93] All nonbonded interactions were considered with 12.0 Å cutoffs and 10.0 Å tapers. The time steps of trajectory integrations were 0.1 fs for the fewest switches surface hopping simulations and 0.5 fs for all others. Multireference quantum chemical calculations were carried out using MOLPRO.[116] All other quantum chemical calculations were performed with developers' version of Q-Chem package[117] linked with NBO 5.0.[118] MD simulations were conducted with GROMACS 4.0.7[119] linked with the in-house libraries for performing diabatic potential energy matrix interpolation and trajectory surface hopping.[24]

3. CHECKING THE RELIABLITIES

Diabatic Electronic Population Matrix. The elements of the atomic diabatic electronic population matrices obtained through our scheme are listed in Table 1, with the atom designations shown in Figure 2. From the definitions of the elements of this matrix, the diagonal elements will correspond to the partial charges of the diabatic states on each atom. In addition, each off-diagonal element will reflect the one-electron character in the transitions between the two corresponding diabatic wave functions within the given atom space.[94] Interestingly, the charge values are state dependent only on heavy atoms. This fact can be explained by the insensitivity of the electronic structure around hydrogen atoms, which implies that the electron population transfers mainly through the heavy atoms upon electronic transitions. The charge migration pattern can be more straightforwardly observed by measuring the group partial charges, defined as the sum of the atomic populations in each group. The group partial charges in the diabatic states are additionally displayed in Table 1. By inspecting these group charges of each moiety, we can judge whether they are in accord with the characteristics of the diabatized states. As explained in the previous section, the three diabatic states denoted as P, I, and B possess the negative charge localized in the phenoxy, the imidazolinone, and the bridge moieties of the *p*HBI anion, respectively.[53] The negative electronic populations are indeed distributed on the parts where more electrons are expected to be localized. For example, the diabatic partial charge on the phenoxy ring is −1.0 *e* in the P state, while it is −0.19 *e* and 0.44 *e* in the I and the B states. We can also probe how charge transfer occurs with the state changes by analyzing the diabatic charges in an atom-by-atom manner. The negative charge is concentrated (larger than −0.1 *e*) on C_2, C_4, C_6, and O_7 atoms in the P state; C_{13}, C_{15}, and O_{18} atoms in the I state; and C_{12} atom in the B state. This is in good agreement with the shapes of the localized orbitals displayed in Figure 3. Therefore, we can see that both the group charges of the individual moieties and the atomic partial charges are in correct accord with the definitions of our diabatic states.

It should also be noted that the off-diagonal population matrix elements are overall rather small except for three atoms, C_4, C_{12}, and C_{13}. In contrast to the on-diagonal elements, which depend only on the characteristics of single diabatic wave functions, the off-diagonal elements are determined by the mutual orientations between the two involved diabatic wave functions. Because the extent to which a pair of localized orbitals overlap on any given atom will change depending on the molecular geometry, these off-diagonal elements will have stronger dependences on geometric distortions than the on-diagonal elements. At least, in this work, the diabatic states are defined based on the Foster−Boys localized orbitals, and the off-diagonal elements tend to be small, somewhat similarly to off-diagonal dipole terms, as in ref 120. Because they are small, the absolute magnitudes do not vary much upon geometrical distortions. Thus, all the diabatic population matrix elements have relatively small geometry dependences, leading to reliable description of electrostatic interactions toward condensed phase simulations in the excited state.

Fixed Diabatic Partial Charge Assumption. To guarantee that employing the diabatic electronic population matrix with fixed charge values is a reliable approach in molecular simulations, we should also verify our assumption of the fixed charges. This is equivalent to assuming that the electronic structures of the diabatic states are invariant to molecular deformations of the chromophore (internal polarization) and to environmental changes around the chromophore (external polarization). The first issue, namely the internal polarization, can be examined by calculating diabatic electronic population matrices at varying chromophore geometries. For this, we have performed the charge diabatizations at the 1500 geometries that were employed as the interpolation

dx.doi.org/10.1021/ct5006856 | J. Chem. Theory Comput. XXXX, XXX, XXX−XXX

data points. Namely, the natural population analysis based formalism was applied to each of the data points to generate partial charges on each atom. Then, the average atomic charge and its variations as represented by the root-mean-squared (rms) deviations within the 1500 values were calculated. These data are shown in Table 2 for the three diabatic states.

Table 2. Diabatic Atomic Partial Charges Averaged over the 1500 Test Geometries, Represented by the Diagonal Elements of the Diabatic Electronic Population Matrices[a]

atom[b]	P		I		B	
C_1	0.527	(0.030)	0.598	(0.021)	0.568	(0.032)
C_2	−0.432	(0.038)	−0.317	(0.028)	−0.314	(0.033)
C_3	−0.183	(0.020)	−0.142	(0.022)	−0.193	(0.027)
C_4	−0.300	(0.085)	−0.044	(0.079)	0.011	(0.074)
C_5	−0.183	(0.018)	−0.143	(0.024)	−0.195	(0.028)
C_6	−0.434	(0.034)	−0.320	(0.028)	−0.315	(0.033)
O_7	−0.823	(0.034)	−0.715	(0.022)	−0.726	(0.027)
H_8	0.218	(0.004)	0.217	(0.004)	0.217	(0.004)
H_9	0.229	(0.014)	0.229	(0.014)	0.229	(0.014)
H_{10}	0.217	(0.004)	0.217	(0.004)	0.217	(0.004)
H_{11}	0.213	(0.008)	0.213	(0.008)	0.213	(0.008)
C_{12}	−0.028	(0.139)	−0.056	(0.160)	−0.640	(0.170)
C_{13}	0.061	(0.074)	−0.245	(0.099)	0.127	(0.081)
N_{14}	−0.547	(0.018)	−0.537	(0.015)	−0.558	(0.016)
C_{15}	0.332	(0.034)	0.155	(0.050)	0.304	(0.035)
N_{16}	−0.741	(0.017)	−0.741	(0.016)	−0.740	(0.017)
C_{17}	0.792	(0.030)	0.667	(0.035)	0.721	(0.030)
O_{18}	−0.723	(0.026)	−0.843	(0.036)	−0.735	(0.032)
H_{19}	0.192	(0.006)	0.192	(0.006)	0.192	(0.006)
H_{20}	0.421	(0.007)	0.421	(0.007)	0.420	(0.007)
H_{21}	0.198	(0.010)	0.198	(0.016)	0.204	(0.011)

[a]The root-mean-squared deviations of the charges are also shown in parentheses. [b]Atom designations are found in Figure 2.

The r.m.s. deviations of the atomic partial charges in each diabatic state are <0.04 *e* except for three atoms (C_4, C_{12}, C_{13}) that form the "flexible" link between the two rings in the excited state. On these three atoms, the deviations are in the 0.07−0.17 *e* range. To judge how large these deviations are in comparison with the same quantities in conventional fixed partial charge models of more regular biomolecules, we have conducted a similar natural population analysis for 1000 ensemble geometries of tryptophan and glutamate side chains at 300 K. We chose these residues as two extreme cases of observing charge deviations: the tryptophan side chain is aromatic and rigid and thus its conformation will not change to any substantial degree, while glutamate is aliphatic and thus will involve a large amount of geometric distortions. The rms deviations of the atomic partial charges of their non-hydrogen atoms are in the ranges 0.01−0.02 *e* for tryptophan and 0.05−0.08 *e* for glutamate. Therefore, we can infer that the geometry dependent deviations from the fixed charge values within our diabatic model with multiple electronic states are roughly twice larger than the deviations from the frequently adopted point charges with single electronic states, in both rigid and flexible parts of the chromophore. Considering the complications associated with the increased number of electronic states and the extended nature of the geometric distortions of the chromophore, it is indeed encouraging to observe that the fixed diabatic partial charges are not excessively more deviating than in other biomolecular cases with single electronic states.

We mentioned that the deviations of the charges on C_4, C_{12}, and C_{13} are fairly larger compared to the other atoms. Besides the fact that these atoms are on the flexible bridge that connects the imidazolinone ring to the phenoxy ring, they will likely be heavily involved during the charge transfer with the electronic excitation. This interpretation is also supported by larger values of the off-diagonal elements of the corresponding diabatic electronic population matrices. Because the virtue of our formalism comes in part from the small magnitudes of the off-diagonal elements and their subsequent insensitivities to geometric distortions, as mentioned in the previous section, the relatively large off-diagonal elements may also reduce the reliability of our formalism. Of course, as the deviations of the diabatic charges on these atoms are still almost comparable with the charge deviations with the flexible group in the conventional force field case, they will still not likely affect the reliability of our fixed diabatic charge assumption at least in the qualitative sense.[58] In this sense, to obtain quantitatively improved characterizations, the internal polarizations of the

Table 3. Adiabatic Charges Back-Transformed from the Diabatic Electronic Population Matrices, In Comparison with the Reference Natural Population Based Charges at Three Critical Geometries

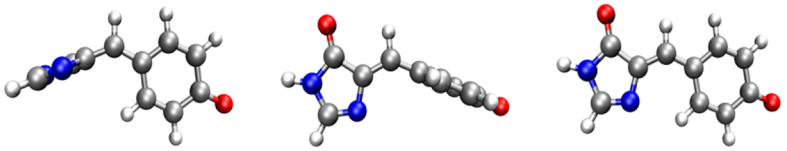

		I-twisted			P-twisted			Planar[a]		
Method	Group[b]	S_0	S_1	S_2	S_0	S_1	S_2	S_0	S_1	S_2
Transformed adiabatic charges	G_P	−0.185	−0.757	−0.687	−0.997	−0.347	−0.285	−0.651	−0.543	−0.435
	G_I	−0.972	−0.317	−0.070	−0.153	−0.715	−0.663	−0.608	−0.505	−0.419
	G_B	0.157	0.074	−0.242	0.150	0.062	−0.051	0.259	0.048	−0.146
NBO charges	G_P	−0.287	−0.770	−0.507	−1.032	−0.113	−0.137	−0.651	−0.543	−0.435
	G_I	−1.020	−0.113	−0.123	−0.273	−0.735	−0.525	−0.608	−0.505	−0.419
	G_B	0.308	−0.090	−0.265	0.306	−0.145	−0.315	0.259	0.048	−0.146

[a]Because the charge diabatization was performed at this planar geometry, the two sets of charges are identical here. [b]Group designations are found in Figure 2.

dx.doi.org/10.1021/ct5006856 | J. Chem. Theory Comput. XXXX, XXX, XXX−XXX

diabatic states (geometric dependence) should be appropriately considered. One possibility will be an adoption of geometry-dependent diabatic charges. We believe that the diabatic electronic population matrix formalism can also be extended for defining geometry-dependent partial charges, especially when it is linked with the interpolation approach. We also note that once the geometry-dependence is introduced, adopting adiabatic partial charge models might become equally plausible. However, because the definitions of the adiabatic states will be affected by the interactions with the external MM charges as shown in Figure 1, we believe the diabatic approach will still be a better option even when the geometric dependence is introduced.

Our current model also neglects the external polarization effect by construction. The polarization of the electron distribution inside the chromophore by external factors will surely affect the partial charges in the chromophore, and should be properly considered for an improved description. In fact, there have been continued successes in improving the parametrizations of the polarization effects of an arbitrary molecule[32−41] for evaluating its polarization energies more reliably.[42−48] We anticipate that these concepts should also be extendable for describing the diabatic states of chromophore molecules. At this stage, we feel that these developments for multiple electronic states are beyond the scope of the present work and leave it as a target of future investigations.

Transformation to Adiabatic Charges. In many situations, the trajectories of dynamics simulations are propagated on adiabatic surfaces. Thus, reliably reproducing the adiabatic charges will be important for trustable simulations. In our scheme, the adiabatic charges will naturally vary with chromophore distortions even though the diabatic electronic population matrices are fixed. Therefore, checking the adiabatic charges at widely varying molecular geometries will also give information on how appropriately our scheme is performing to represent the electrostatic property of the chromophore molecule. Toward this end, we have selected two representatively twisted molecular geometries as displayed with the figure panels in Table 3, with the twists imposed through the imidazolinone and the phenoxy channels. For brevity, we will respectively denote these as the I-twisted and the P-twisted conformations. Because *p*HBI after photoexcitation twists through these channels and quenches nonadiabatically to the S_0 state, the capability of reproducing the adiabatic charges at these geometries will be crucial for performing reliable nonadiabatic simulations.

The adiabatic group charges obtained by transforming the diabatic charges are listed in Table 3, together with the matching reference quantum chemical values as obtained by analyzing natural populations with the adiabatic wave functions. One can clearly see that the adiabatic charges from our scheme are generally in good agreements with the reference values, with its average and maximum deviations respectively at the ∼0.15 *e* and ∼0.30 *e* levels. Considering that 2−11 atoms form each group, these deviations are at reasonably similar levels to what we have already observed in the previous part with the atomic deviations. It also implies that the errors will likely be stemming from the limitations of the fixed charge model. Thus, we can see that the adiabatic charges can be generated from the diabatic charges reliably enough. Also, because the selected geometries in this test are within the "small gap energy region" with excitation energies smaller than 1 eV, the adiabatized charges in the conical intersection region will likely be similarly reliable.

We also note that our charge distribution is in good accord with the characteristics of a related chromophore, *para*-hydroxybenzylidiene-1,2-dimethyl-imidazolin-5-one (*p*HBDI). Our analyses show that when *p*HBI takes the I-twisted form, the negative charge is majorly distributed on the imidazolinone ring in the S_0 state and on the phenoxy ring in the S_1 state. On the other hand, at the P-twisted geometry, the negative charge concentrates to the phenoxy ring in the S_0 state, while it transfers to the imidazolinone ring in the S_1 state. These aspects agree very favorably with the characteristics of the GFP chromophore analogue *p*HBDI, as reported by Olsen et al.[53]

Up to this point, we have discussed the performance of our diabatic electronic population matrix scheme on evaluating atomic partial charges. The diabatic partial charges described the properties of diabatic states reasonably well, and they did not vary too much upon geometric distortions. The off-diagonal elements, which intrinsically have some geometry dependences, were actually quite small in their magnitudes and also did not vary too much with different chromophore geometries. The level of reliability of the fixed charge model was shown to be comparable to that of more conventional and widely adopted fixed point charge models of biomolecules with single electronic states. As a consequence, the reverse-transformed adiabatic charges also agreed reasonably well with the quantum chemically calculated reference values at geometries that are close enough to conical intersections. These observations indicate that the fixed diabatic electronic population model can be applied to evaluating electrostatic energies between the chromophore and its environment for simulating nonadiabatic dynamics. Before moving on to such actual simulations of dynamics, let us investigate how accurately the electrostatic interaction energies can indeed be calculated.

Energy Evaluations with Diabatic Electronic Population Matrix. We have stated that the electrostatic interaction energy between the chromophore and its environment will be evaluated more accurately by employing the fixed *diabatic* partial charges than by adopting fixed *adiabatic* charges. To elucidate the degree of improvement, as mentioned in a previous section, 2000 snapshots of the solvated *p*HBI anion were generated from 500 independent MD trajectories of 3.0 ps durations on the S_1 surface, and then, they were adopted to calculate the Coulombic interaction energies within the framework of IM/MM with fixed diabatic partial charges. These were then compared with the interaction energies from IM/MM with fixed adiabatic partial charges, and with the matching energies from QM/MM. Of course, the QM/MM results can be regarded as the references for comparisons.

This type of analysis requires a scheme that can measure the chromophore-environment electrostatic interaction (denoted as IM:MM or QM:MM interaction) separately from the environment-environment interaction (MM:MM interaction). This is achieved in the following manner. For a given chromophore-environment conformation in the ground state, let us consider

$$\Delta E^{S_0} = E^{S_0}_{IM/MM} - E^{S_0}_{IM} \tag{29}$$

where the two terms on the right-hand side are the total system energy and the chromophore-only energy from interpolation, respectively. This energy difference will include IM:MM and MM:MM interaction terms, with the latter likely dominating in magnitude due to the larger number of particles involved. When the same energy difference in the S_1 state is additionally considered and the double energy difference is generated as

dx.doi.org/10.1021/ct5006856 | J. Chem. Theory Comput. XXXX, XXX, XXX−XXX

$$\Delta\Delta E = \Delta E^{S_1} - \Delta E^{S_0} = (E^{S_1}_{IM/MM} - E^{S_1}_{IM}) - (E^{S_0}_{IM/MM} - E^{S_0}_{IM}) \quad (30)$$

the MM:MM contribution will simply cancel out. As it is independent of the MM:MM interaction with the nonpolarizable MM condition, we can adopt $\Delta\Delta E$ as a metric for quantifying the pure IM:MM interaction term. The same double energy difference can of course be calculated within electrostatically embedded QM/MM. In addition, this double energy difference is actually equivalent to the change from the chromophore-only excitation energy ($E^{S_1}_{IM} - E^{S_0}_{IM}$) to the total system excitation energy ($E^{S_1}_{IM/MM} - E^{S_0}_{IM/MM}$) and will reflect how the external MM particles perturb the excited state and the ground state to vary the excitation gap in between.

Figure 4 shows the $\Delta\Delta E$ values at the 2000 test geometries with the fixed adiabatic and the fixed diabatic charges in comparison with the QM/MM results. Not surprisingly, $\Delta\Delta E$ computed with the adiabatic partial charges displays poor correlation with the reference. Interestingly, many points appear on a horizontally flat line. The aspect can be understood from the fact that the fixed adiabatic charge does not change upon chromophore conformational distortions. Namely, the $\Delta\Delta E$ values computed with the adiabatic charge model will be largely independent of the chromophore conformational changes, while the $\Delta\Delta E$ from QM/MM will be strongly affected by it. On the contrary, $\Delta\Delta E$ values computed with diabatic charges have good correlation with the QM/MM results. Therefore, we can infer that our scheme with the fixed diabatic electronic population matrix is recovering the chromophore geometry dependence of the electrostatic interactions, at least in a qualitatively correct manner.

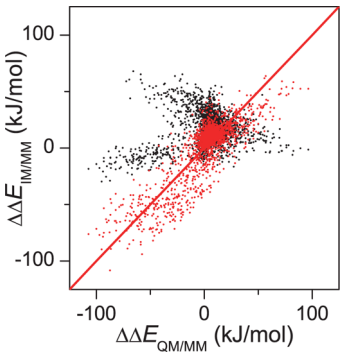

Figure 4. $\Delta\Delta E$ (eq 30) at the 2000 test geometries generated with the diabatic electronic population matrix formalism (red dots) and with the fixed adiabatic partial charges (black dots), in comparison with the reference QM/MM values. For comparison, a perfect correlation line is drawn in red along the diagonal.

Even still, we should expect a certain level of discrepancy between our diabatic charge based IM/MM estimations and QM/MM references. This is mainly caused by the two polarization effects that we have already described in a previous part. With our scheme, we do include the geometric dependence of the adiabatic charges but neglect the dependence of the diabatic charges (internal polarization). In addition, even the wave function and the orbitals at a fixed geometry of the IM part should be perturbed by the external MM charges (external polarization).[32−48] In the electrostatically embedded QM/MM case, these internal and external polarizations are naturally included except the repolarization effect on the QM area by the missing polarization of the MM environment. Nevertheless, our scheme with the fixed charge approximation still yields fairly good agreements with QM/MM as depicted in Figure 4, and it will likely produce qualitatively or semiquantitatively correct simulation results. Of course, its reliability will improve if the two polarization effects can be additionally considered in appropriate manners in the future.

4. DEMONSTRATIONS WITH MOLECULAR SIMULATIONS

Simulations of Nonadiabatic Dynamics. Our scheme can become really meaningful when it is applied to molecular simulations with long enough durations in sufficiently large ensembles. To demonstrate such an aspect, we have conducted nonadiabatic surface hopping simulations of a solvated *p*HBI anion with our diabatic charge model in conjunction with the interpolation scheme, by adopting the fewest switches and the Landau−Zener hopping formalisms as mentioned in a previous section. We have adopted both the single-level and the dual-level interpolations for the chromophore internal potentials.

From the simulation data, we monitored nonadiabatic population decay patterns from the S_1 state. These decay patterns with the four combinations of simulation methods are presented in Figure 5 along with their decay time coefficients listed in Table 4. The time scales of the population decays obtained from bare chromophore simulations in the gas phase are also listed in this table for comparison. Because the QM/MM simulations with multiple trajectories are excessively time-consuming, directly comparing all our results to QM/MM references is not feasible. Instead, we performed one short set of QM/MM Landau−Zener hopping simulations over 0.25 ps, starting from 100 solvated structures. Of course, the details of QM and MM conditions exactly matched those in the IM/MM simulations. As shown in the inset of Figure 5, the population decay pattern with the reference QM/MM trajectories agrees very well with the corresponding IM/MM result.

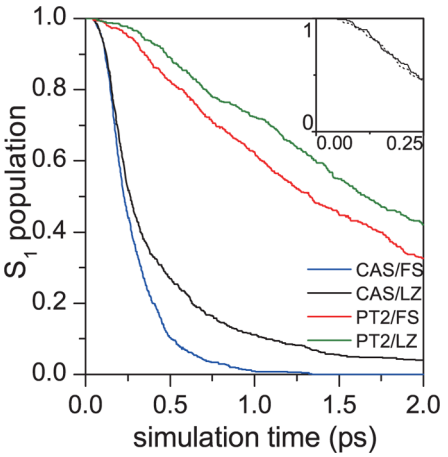

Figure 5. S_1 population decays in time from nonadiabatic dynamics simulations with the diabatic charges. CAS and PT2 denote the QM methods utilized for constructing the interpolation data sets, namely SA3-CAS(4,3) and SA3-CAS(4,3)-PT2. FS and LZ correspond to the fewest switches and the Landau−Zener type surface hopping algorithms, respectively. The inset compares the CAS/LZ population decays calculated with the IM/MM (solid) and the QM/MM (dashed) approaches.

dx.doi.org/10.1021/ct5006856 | J. Chem. Theory Comput. XXXX, XXX, XXX−XXX

Table 4. Simulated Non-Radiative Decay Time Scales of *p*HBI

simulation set	level of theory[a]	SH scheme[b]	τ(ps)[c]
gas phase	SA3-CAS(4,3)	FS	1.03[d]
	SA3-CAS(4,3)-PT2	FS	3.04[d]
aqueous solvation	SA3-CAS(4,3)	FS	0.29
		LZ	0.43
	SA3-CAS(4,3)-PT2	FS	2.00
		LZ	2.70

[a]Ab initio level of theory employed in constructing the interpolation data set. [b]Surface hopping schemes utilized in the nonadiabatic simulations: fewest switches surface hopping (FS) and Landau−Zener type surface hopping (LZ). [c]Time scales were obtained by fitting the data in Figure 5 to a single exponential decay function, $f = \exp(-t/\tau)$. [d]Values taken from ref 93.

With the nonadiabatic simulations, we can observe the extent to which the electrostatic interactions affect the surface crossing dynamics. From Table 4, we can see that the electrostatic effects from aqueous solvation consistently expedite the nonradiative deactivation from the excited state in all combinations of the simulation protocols. This change of population transfer rate compares favorably with the previously reported population dynamics obtained with QM/MM or semiempirical quantum chemical calculations.[3,51] In fact, this expedition also compares somewhat interestingly with Figure 4. We have noted that $\Delta\Delta E$ in the figure represents whether the solvation increases or decreases the $S_1 - S_0$ gap (eq 30). Because the gap decreases ($\Delta\Delta E < 0$) only in a limited fraction of the tested geometries and because a smaller gap will make the nonadiabatic transition faster, we can infer that this limited fraction actually has dominance over the decay dynamics. When we inspected the conditions of seeing negative $\Delta\Delta E$ values, we indeed observed that smaller $S_1 - S_0$ gaps (namely, small excitation energies) were strongly related with the negativity of $\Delta\Delta E$ (Figure S1 in Supporting Information). This feature further supports that the small fraction of conformations with decreasing gap energies with solvation indeed shortens the time scale of the nonadiabatic transition.

Also, it is interesting to note that the Landau−Zener hopping simulations yielded quite similar population decay patterns to the more sophisticated fewest-switches simulation results. In addition, when we tried different cutoff energies for trajectory hopping, we observed rather small changes in the decay patterns and time scales. Because of its reduced computational cost, Landau−Zener simulations have in fact been often used in studying photophysics of proteins via the ab initio direct dynamics.[4,59,113,121] Even though a caution should be taken against judging only with the population transfer rate of *p*HBI, our simulation results still signal that the Landau−Zener type formalism may be utilized in studying excited state dynamics of complex systems as an economic alternative to more expensive and elaborate tools, just as in the previous studies mentioned above. Of course, the IM/MM scheme will make it possible to compare the two approaches directly with more examples and more metrics.

Dynamic Stokes Shift and Solvent Dynamics. As mentioned in the above, the dynamics of nonadiabatic transitions are closely related to the gap energy between the two involved states and its change in time. Its change in the ensemble sense, which is often termed as the dynamic Stokes shift,

$$S(t) = \overline{\Delta E(t)} - \overline{\Delta E(0)} \tag{31}$$

is also a key quantity in describing the dynamics of electronically excited system in the condensed phase.[8,50,93,122−135] Here, $\overline{\Delta E(t)}$ is an ensemble average of the gap energy at time t. Before concluding, let us discuss the system (namely, both the chromophore and its environment) dynamics after electronic transition in terms of this dynamic Stokes shift with our diabatic electronic population matrix formalism. The response of solvent molecules (and/or protein side chains if the chromophore is embedded in a protein)[136] upon a sudden change in the electron distribution of the chromophore tends to dominate the dynamic Stokes shift,[127−130] potentially after very fast intramolecular vibrational relaxation in the chromophore.[8,137] Many previous MD studies on such dynamics have modeled electronic excitations as changes in the chromophore atomic partial charges,[8,50,93,122−129] and have successfully explained the solvent-related dynamics. Following the solute or the chromophore dynamics will likely require a more advanced modeling scheme. The case with a chromophore such as *p*HBI will be in such a situation, where the electronic transition forces a large molecular distortion, which then again alter the electron distribution in a twisting pathway dependent manner. In fact, in *p*HBI with our model, the atomic charges change more along the twisting pathways on the S_1 surface than they change upon the vertical $S_0 \rightarrow S_1$ electronic transition. (See Table 3.) Our diabatic electronic population matrix formalism can represent its basic nature in the qualitative sense, as it can describe the geometry dependent charge changes of the chromophore in the adiabatic states. Therefore, comparing the behaviors with the present diabatic and the conventional adiabatic charge models may present intriguing information.

Toward this end, we have conducted 500 independent single electronic state MD simulations on the S_1 surface of 3.0 ps durations using the *NPT* condition and calculated the dynamic Stokes shift $S(t)$ by taking the time-dependent averages of the gap energies over the trajectories. Vertical transitions from an equilibrium ensemble in the S_0 state were assumed as the initial conditions of the trajectories. Figure 6a presents how the dynamic Stokes shift appears with the two different charge models. Indeed, the overall decay patterns are quite different. Not surprisingly, when $S(t)$ is decomposed into the chromophore internal energy contribution (namely, the interpolated energy; $S_{int}(t)$) and the Coulombic contribution (the IM:MM term; $S_{elec}(t)$), as respectively displayed in Figure 6b and c, it can be seen that the discrepancy is caused majorly by the difference in the Coulombic contributions. The internal energy of the solute molecule, which shifts by 180 kJ/mol at t = 3 ps, offers a major part of the dynamic Stokes shift in both cases. This signifies that the solute molecule relaxes its excess vibrational energy after the vertical Franck−Condon transition by following the two available twisting pathways in a manner that is somewhat independent of the Coulombic interactions with water. However, there still is an apparent difference in the decay patterns from the two models in Figure 6b and the detailed relaxation dynamics differs with different electrostatic interactions. Compared to this rather fast vibrational relaxation, the shift from the Coulombic contribution varies quite slowly with the diabatic charge model. The magnitude of the shift is also much smaller than with the adiabatic charge model. Interestingly, the shift itself with the adiabatic charge finishes much more quickly. All these differences between the two

dx.doi.org/10.1021/ct5006856 | J. Chem. Theory Comput. XXXX, XXX, XXX−XXX

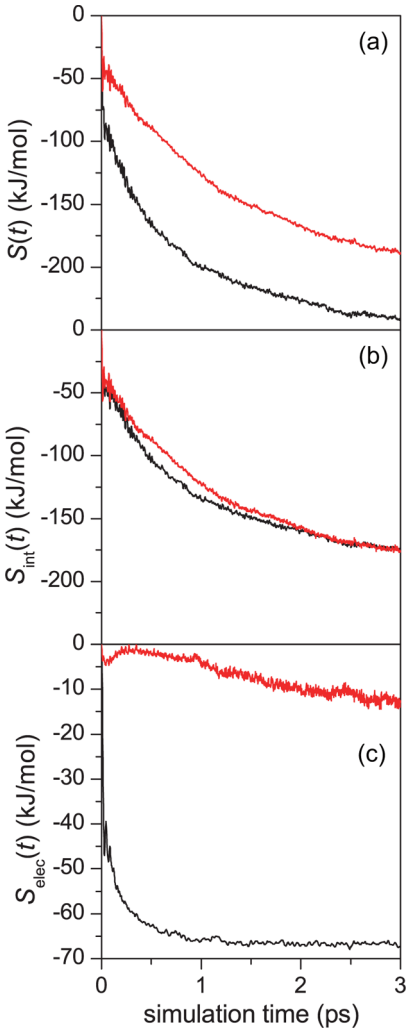

Figure 6. (a) Simulated dynamic Stokes shift of *p*HBI in water, and its decomposition into (b) the chromophore internal energy contribution and (c) the chromophore−solvent Coulombic interaction contribution. The red lines represent the results with the diabatic electronic population matrix formalism while the black lines display the results with the fixed adiabatic charges.

charge models are caused by the exaggerations in the atomic charges with the adiabatic model. As already explained, the adiabatic charges in the S_0 and the S_1 states were fitted at the most stable geometries in each state. Thus, the negative charge was concentrated on the imidazolinone and the phenoxy rings in the S_0 state with a planar geometry, while it was localized on the imidazolinone ring and the bridge in the S_1 state with a P-twisted conformation. With the fixed adiabatic model, in the S_1 state, the imidazolinone ring and the bridge still possess large amounts of negative charge even at the planar Franck−Condon geometry. On the contrary, the diabatic partial charges were modeled at the Franck−Condon geometry, and such an exaggeration did not occur by construction. Indeed, the reason we chose the S_0 geometry as the reference point of finding the fixed diabatic electronic population matrices was to minimize an unphysical relaxation effect right after the photoexcitation from the stable ground state ensemble.

The fact that the Coulomb component of the shift, namely $S_{elec}(t)$, with the adiabatic charge flattens much more quickly (Figure 6c) can also be explained with the same argument. As can be seen in the figure, $S_{elec}(t)$ converges in a very short time (~500 fs) with the simulations with adiabatic charges. On the contrary, $S_{elec}(t)$ decays continuously up to 3.0 ps in simulations with the diabatic charge model. As noted in previous parts, our diabatic model generates geometry-dependent atomic charges after readiabatizations. Thus, the electrostatic interactions between the chromophore and the solvent during the simulations varies following the conformational changes of the chromophore, and the Coulombic component of the dynamic Stokes shift will continuously be affected by the chromophore relaxation. This view is also supported by our simulations, which show that the chromophore twisting also occurs in ~3 ps (Figure S2 in Supporting Information). Because the atomic partial charges are fixed in the adiabatic charge model regardless of the chromophore geometry, the Coulombic contribution does not have a lasting effect on $S(t)$. This suggests that studying resolvation dynamics of chromophores with large Stokes shifts and excited state surface crossings will require models that can describe the geometry dependent nature of the charge distributions. Our model with the diabatic electronic population matrix formalism can indeed fulfill such a requirement at least at a basic level.

5. CONCLUDING REMARKS

In this article, we have introduced the concept of the diabatic electronic population matrix and demonstrated its application to the excited state simulations of *p*HBI. To compute the diabatic electronic populations of the chromophore, we first have generated the adiabatic electronic population matrices in the atomic subspaces by adopting the natural population formalism. These were then unitary transformed to form the electronic populations in the diabatic states. The obtained diabatic atomic charges preserved the characteristics of the diabatic surfaces with reasonably small dependences on nuclear displacements. The backward-transformed adiabatic charges correctly described the electron localizations in the corresponding adiabatic states at critical geometries. Also, when the fixed diabatic charge model was combined with the interpolation scheme for the chromophore internal energy description, the contribution by the chromophore-environment interaction toward the excitation energy was described more reliably than with the fixed adiabatic charge model. We demonstrated that the fixed diabatic electronic population matrix formalism can be readily employed in trajectory simulations both in the nonadiabatic and adiabatic conditions. The simulation results compared very favorably with the QM/MM results at least in the case where the comparison was practically feasible. In nonadiabatic simulations, the fewest switches and the Landau−Zener hopping approaches yielded similar population decay patterns, supporting the view that the Landau−Zener scheme can be adopted as an economic alternative for investigating nonadiabatic phenomena in complex systems. The dynamic interplay between the chromophore conformation change and the subsequent relaxation of the Coulombic interaction was also revealed by utilizing simulations with our diabatic electronic population matrix formalism.

Although the energy calculations using diabatic electronic population matrix presented here compares favorably with the results from QM/MM, there are still apparent limitations. First, dispersive interactions are not included in diabatization. In fact, the dispersive property of a molecule will also depend on the diabatic states, and its parameters should be obtained accordingly. Including variations of the electrostatic interactions from the internal and external polarization effects will also

dx.doi.org/10.1021/ct5006856 | J. Chem. Theory Comput. XXXX, XXX, XXX−XXX

improve the accuracies of interaction energy calculations. Of course, the deviation of the pseudodiabatization scheme from mathematical perfectness will additionally affect the reliability. Nonetheless, our results show that the description of the excited state and the ground state energetics of the chromophore molecule is improved within our fixed charge formalism, and our model will be useful for reliably describing electrostatic interactions in situations with multiple electronic states. Studies on the dynamics of photoproteins with our diabatic electronic population matrix formalism in combination with the interpolation scheme are in progress now and will be reported in due course.

■ ASSOCIATED CONTENT

Ⓢ Supporting Information

Complete refs 42, 116, and 117, relationships between the S_0-S_1 gap energy and $\Delta\Delta E$, and the simulated time progress of the bridge dihedral angles of *p*HBI. This material is available free of charge via the Internet at http://pubs.acs.org.

■ AUTHOR INFORMATION

Corresponding Author

*E-mail: ymrhee@postech.ac.kr.

Notes

The authors declare no competing financial interest.

■ ACKNOWLEDGMENTS

This work was supported by the Institute for Basic Science (IBS) in Korea. The supercomputer time from Korea Institute of Science and Technology Information (KISTI) is also gratefully acknowledged.

■ REFERENCES

(1) Allen, M. P.; Tildesley, D. J. *Computer Simulation of Liquids*; Oxford University Press: Oxford, 1987.

(2) Frenkel, D.; Smit, B. *Understanding Molecular Simulation*; Academic Press: London, 2002.

(3) Virshup, A. M.; Punwong, C.; Pogorelov, T. V.; Lindquist, B. A.; Ko, C.; Martínez, T. J. Photodynamics in Complex Environments: Ab Initio Multiple Spawning Quantum Mechanical/Molecular Mechanical Dynamics. *J. Phys. Chem. B* **2009**, *113*, 3280−3291.

(4) Li, X.; Chung, L. W.; Mizuno, H.; Miyawaki, A.; Morokuma, K. Primary Events of Photodynamics in Reversible Photoswitching Fluorescent Protein Dronpa. *J. Phys. Chem. Lett.* **2010**, *1*, 3328−3333.

(5) Park, J. W.; Rhee, Y. M. Interpolated Mechanics-Molecular Mechanics Study of Internal Rotation Dynamics of the Chromophore Unit in Blue Fluroescent Protein and Its Variants. *J. Phys. Chem. B* **2012**, *116*, 11137−11147.

(6) Nguyen, K. A.; Rossi, I.; Truhlar, D. G. A Dual-Level Shepard Interpolation Method for Generating Potential Energy Surfaces for Dynamics Calculations. *J. Chem. Phys.* **1995**, *103*, 5522−5530.

(7) Rhee, Y. M. Construction of an Accurate Potential Energy Surface by Interpolation with Cartesian Weighting Coordinates. *J. Chem. Phys.* **2000**, *113*, 6021−6024.

(8) Park, J. W.; Kim, H. W.; Song, C.-I.; Rhee, Y. M. Condensed Phase Molecular Dynamics Using Interpolated Potential Energy Surfaces with Application to the Resolvation Process of Coumarin 153. *J. Chem. Phys.* **2011**, *135*, 014107.

(9) Jordan, M. J. T.; Thompson, K. C.; Collins, M. A. Convergence of Molecular Potential Energy Surfaces by Interpolation: Application to the OH + H_2 → H_2O + H Reaction. *J. Chem. Phys.* **1995**, *102*, 5647−5657.

(10) Jordan, M. J. T.; Thompson, K. C.; Collins, M. A. The Utility of Higher Order Derivatives in Constructing Molecular Potential Energy Surfaces by Interpolation. *J. Chem. Phys.* **1995**, *103*, 9669−9675.

(11) Jordan, M. J. T.; Collins, M. A. An Interpolated Unrestricted Hartree−Fock Potential Energy Surface for the OH + H_2 → H_2O + H Reaction. *J. Chem. Phys.* **1996**, *104*, 4600−4610.

(12) Bettens, R. P. A.; Hansen, T. A.; Collins, M. A. Interpolated Potential Energy Surface and Reaction Dynamics for $O(^3P)$ + H_3^+ $(^1A_1')$ and $OH^+(^3\Sigma^-)$ + $H_2(^1\Sigma g^+)$. *J. Chem. Phys.* **1999**, *111*, 6322−6332.

(13) Collins, M. A.; Zhang, D. H. Application of Interpolated Potential Energy Surfaces to Quantum Reactive Scattering. *J. Chem. Phys.* **1999**, *111*, 9924−9931.

(14) Moyano, G. E.; Collins, M. A. Molecular Potential Energy Surfaces by Interpolation: Strategies for Faster Convergence. *J. Chem. Phys.* **2004**, *121*, 9769−9775.

(15) Moyano, G. E.; Pearson, D.; Collins, M. A. Interpolated Potential Energy Surfaces and Dynamics for Atom Exchange between H and H_3^+, and D and H_3^+. *J. Chem. Phys.* **2004**, *121*, 12396−12401.

(16) Collins, M. A. Molecular Potential Energy Surfaces Constructed from Interpolation of Systematic Fragment Surfaces. *J. Chem. Phys.* **2007**, *127*, 024104.

(17) Ischtwan, J.; Collins, M. A. Molecular Potential Energy Surfaces by Interpolation. *J. Chem. Phys.* **1994**, *100*, 8080−8088.

(18) Evenhuis, C. R.; Collins, M. A. Locally Optimized Coordinates in Modified Shepard Interpolation. *J. Phys. Chem. A* **2009**, *113*, 3979−3987.

(19) Thompson, K. C.; Jordan, M. J. T.; Collins, M. A. Polyatomic Molecular Potential Energy Surfaces by Interpolation in Local Internal Coordinates. *J. Chem. Phys.* **1998**, *108*, 8302−8316.

(20) Thompson, K. C.; Jordan, M. J. T.; Collins, M. A. Molecular Potential Energy Surfaces by Interpolation in Cartesian Coordinates. *J. Chem. Phys.* **1998**, *108*, 564−578.

(21) Godsi, O.; Collins, M. A.; Peskin, U. Quantum Grow—A Quantum Dynamics Sampling Approach for Growing Potential Energy Surfaces and Nonadiabatic Couplings. *J. Chem. Phys.* **2010**, *132*, 124106.

(22) Evenhuis, C. R.; Collins, M. A. Interpolation of Diabatic Potential Energy Surfaces. *J. Chem. Phys.* **2004**, *121*, 2515−2527.

(23) Godsi, O.; Evenhuis, C. R.; Collins, M. A. Interpolation of Multidimensional Diabatic Potential Energy Matrices. *J. Chem. Phys.* **2006**, *125*, 104105.

(24) Park, J. W.; Rhee, Y. M. Constructing Polyatomic Potential Energy Surfaces by Interpolating Diabatic Hamiltonian Matrices with Demonstration on Green Fluorescent Protein Chromophore. *J. Chem. Phys.* **2014**, *140*, 164112.

(25) Evenhuis, C. R.; Martínez, T. J. A Scheme to Interpolate Potential Energy Surfaces and Derivative Coupling Vectors without Performing a Global Diabatization. *J. Chem. Phys.* **2011**, *135*, 224110.

(26) Jorgensen, W. L.; Maxwell, D. S.; Tirado-Rives, J. Development and Testing of the OPLS All-Atom Force Fields on Conformational Energetics and Properties of Organic Liquids. *J. Am. Chem. Soc.* **1996**, *118*, 11225.

(27) Reed, A. E.; Weinstock, R. B.; Weinhold, F. Natural Population Analysis. *J. Chem. Phys.* **1985**, *83*, 735−746.

(28) Damm, W.; Halgren, T. A. Polarizable Force Fields. *Curr. Opin. Struct. Biol.* **2001**, *11*, 236−242.

(29) Warshel, A.; Kato, M.; Pisliakov, A. V. Polarizable Force Fields: History, Test Cases, and Prospects. *J. Chem. Theory Comput.* **2007**, *3*, 2034−2045.

(30) Wang, L.-P.; Chen, J.; Van Voorhis, T. Systematic Parametrization of Polarizable Force Fields from Quantum Chemistry Data. *J. Chem. Theory Comput.* **2012**, *9*, 452−460.

(31) Wang, L.-P.; Head-Gordon, T.; Ponder, J. W.; Ren, P.; Chodera, J. D.; Eastman, P. K.; Martínez, T. J.; Pande, V. S. Systematic Improvement of a Classical Molecular Model of Water. *J. Phys. Chem. B* **2013**, *117*, 9956−9972.

(32) Kim, H. W.; Rhee, Y. M. Molecule-Specific Determination of Atomic Polarizabilities with the Polarizable Atomic Multipole Model. *J. Comput. Chem.* **2012**, *33*, 1662−1672.

(33) Nakagawa, S.; Kosugi, N. Polarized One-Electron Potentials Fitted by Multicenter Polarizabilities and Hyperpolarizabilities. Ab

Initio SCF-CI Calculation of Water. *Chem. Phys. Lett.* **1993**, *210*, 180−186.
(34) Kaminski, G. A.; Stern, H. A.; Berne, B. J.; Friesner, R. A. Development of an Accurate and Robust Polarizable Molecular Mechanics Force Field from Ab Initio Quantum Chemistry. *J. Phys. Chem. A* **2004**, *108*, 621−627.
(35) Elking, D.; Darden, T.; Woods, R. J. Gaussian Induced Dipole Polarization Model. *J. Comput. Chem.* **2007**, *28*, 1261−1274.
(36) Chipot, C.; Dehez, F.; Ángyán, J.; Millot, C.; Orozco, M.; Luque, F. J. Alternative Approaches for the Calculation of Induction Energies: Characterization, Effectiveness, and Pitfalls. *J. Phys. Chem. A* **2001**, *105*, 11505−11514.
(37) Celebi, N.; Ángyán, J.; Dehez, F.; Millot, C.; Chipot, C. Distributed Polarizabilities Derived from Induction Energies: A Finite Perturbation Approach. *J. Chem. Phys.* **2000**, *112*, 2709−2717.
(38) Dehez, F.; Ángyán, J. G.; Gutiérrez, I. S.; Luque, F. J.; Schulten, K.; Chipot, C. Modeling Induction Phenomena in Intermolecular Interactions with an Ab Initio Force Field. *J. Chem. Theory Comput.* **2007**, *3*, 1914−1926.
(39) Soteras, I.; Curutchet, C.; Bidon-Chanal, A.; Dehez, F.; Ángyán, J. G.; Orozco, M.; Chipot, C.; Luque, F. J. Derivation of Distributed Models of Atomic Polarizability for Molecular Simulations. *J. Chem. Theory Comput.* **2007**, *3*, 1901−1913.
(40) Gagliardi, L.; Lindh, R.; Karlström, G. Local Properties of Quantum Chemical Systems: The LoProp Apparoach. *J. Chem. Phys.* **2004**, *121*, 4494−4500.
(41) Misquitta, A. J.; Stone, A. J. Distributed Polarizabilities Obtained Using a Constrained Density-Fitting Algorithm. *J. Chem. Phys.* **2006**, *124*, 024111.
(42) Ponder, J. W.; Wu, C.; Ren, P.; Pande, V. S.; Chodera, J. D.; Schneiders, M. J.; Haque, I.; Mobley, D. L.; Lambrecht, D. S.; DiStasio, R. A., Jr.; et al. Current Status of the AMOEBA Polarizable Force Field. *J. Phys. Chem. B* **2010**, *114*, 2549−2564.
(43) Cieplak, P.; Caldwell, J.; Kollman, P. Molecular Mechanical Models for Organic and Biological Systems Going Beyond the Atom Centered Two Body Additive Approximation: Aqueous Solution Free Energies of Methanol and N-methyl Acetamide, Nucleic Acid Base, and Amide Hydrogen Bonding and Chloroform/Water Partition Coefficients of the Nucleic Acid Bases. *J. Comput. Chem.* **2001**, *22*, 1048−1057.
(44) Wang, Z.-X.; Zhang, W.; Wu, C.; Lei, H.; Cieplak, P.; Duan, Y. Strike a Balance: Optimization of Backbone Torsion Parameters of AMBER Polarizable Force Field for Simulations of Proteins and Peptides. *J. Comput. Chem.* **2006**, *27*, 781−790.
(45) Gresh, N.; Cisneros, G. A.; Darden, T. A.; Piquemal, J.-P. Anisotropic, Polarizable Molecular Mechanics Studies of Inter- and Intramolecular Interactions and Ligand−Macromolecule Complexes. A Bottom-up Strategy. *J. Chem. Theory Comput.* **2007**, *3*, 1960−1986.
(46) Xie, W.; Pu, J.; MacKerell, A. D., Jr.; Gao, J. Development of a Polarizable Intermolecular Potential Function (PIPF) for Liquid Amides and Alkanes. *J. Chem. Theory Comput.* **2007**, *3*, 1878−1889.
(47) Holt, A.; Karlström, G. Inclusion of the Quadrupole Moment when Describing Polarization. The Effect of the Dipole−Quadrupole Polarizability. *J. Comput. Chem.* **2008**, *29*, 2033−2038.
(48) Kaminski, G. A.; Stern, H. A.; Berne, B. J.; Friesner, R. A.; Cao, Y. X.; Murphy, R. B.; Zhou, R.; Halgren, T. A. Development of a Polarizable Force Field for Proteins via Ab Initio Quantum Chemistry: First Generation Model and Gas Phase Tests. *J. Comput. Chem.* **2002**, *23*, 1515−1531.
(49) Song, C.-I.; Rhee, Y. M. Development of Force Field Parameters for Oxyluciferin on its Electronic Ground and Excited States. *Int. J. Quantum Chem.* **2011**, *111*, 4091−4105.
(50) Song, C.-I.; Rhee, Y. M. Dynamics on the Electronically Excited State Surface of the Bioluminescent Firefly Luciferase−Oxyluciferin System. *J. Am. Chem. Soc.* **2011**, *133*, 12040−12049.
(51) Toniolo, A.; Olsen, S.; Manohar, L.; Martínez, T. J. Conical Intersection Dynamics in Solution: The Chromophore of Green Fluorescent Protein. *Faraday Discuss.* **2004**, *127*, 149−163.
(52) Olsen, S.; Smith, S. C. Bond Selection in the Photoisomerization Reaction of Anionic Green Fluorescent Protein and Kindling Fluorescent Protein Chromophore Models. *J. Am. Chem. Soc.* **2008**, *130*, 8677−8689.
(53) Olsen, S.; McKenzie, R. H. A Diabatic Three-State Representation of Photoisomerization in the Green Fluorescent Protein Chromophore. *J. Chem. Phys.* **2009**, *130*, 184302.
(54) Olsen, S.; Lamothe, K.; Martínez, T. J. Protonic Gating of Excited-State Twisting and Charge Localization in GFP Chromophores: A Mechanistic Hypothesis for Reversible Photoswitching. *J. Am. Chem. Soc.* **2010**, *132*, 1192−1193.
(55) Bravaya, K. B.; Grigorenko, B. L.; Nemukhin, A. V.; Krylov, A. I. Quantum Chemistry Behind Bioimaging: Insights from Ab Initio Studies of Fluorescent Proteins and Their Chromophores. *Acc. Chem. Res.* **2012**, *45*, 265−275.
(56) Cui, G.; Lan, Z.; Thiel, W. Intramolecular Hydrogen Bonding Plays a Crucial Role in the Photophysics and Photochemistry of the GFP Chromophore. *J. Am. Chem. Soc.* **2012**, *134*, 1662−1672.
(57) Bravaya, K. B.; Khrenova, M. G.; Grigorenko, B. L.; Nemukhin, A. V.; Krylov, A. I. Effect of Protein Environment on Electronically Excited and Ionizaed States of the Green Fluorescent Protein Chromophore. *J. Phys. Chem. B* **2011**, *115*, 8296−8303.
(58) Basma, M.; Sundara, S.; Çalgan, D.; Vernali, T.; Woods, R. J. Solvated Ensemble Averaging in the Calculation of Partial Atomic Charges. *J. Comput. Chem.* **2001**, *22*, 1125−1137.
(59) Boggio-Pasqua, M.; Burmeister, C. F.; Robb, M. A.; Groenhof, G. Photochemical Reactions in Biological Systems: Probing the Effect of the Environment by Means of Hybrid Quantum Chemistry/Molecular Mechanics Simulations. *Phys. Chem. Chem. Phys.* **2012**, *14*, 7912−7928.
(60) May, V.; Kühn, O. *Charge and Energy Transfer Dynamics in Molecular Systems*; John Wiley & Sons: Chichester, 2011.
(61) Jonasson, G.; Teuler, J.-M.; Vallverdu, G.; Mérola, F.; Ridard, J.; Lévy, B.; Demachy, I. Excited State Dynamics of the Green Fluorescent Protein on the Nanosecond Time Scale. *J. Chem. Theory Comput.* **2011**, *7*, 1990−1997.
(62) Pacher, T.; Cederbaum, L. S.; Köppel, H. Approximately Diabatic States from Block Diagonalization of the Electronic Hamiltonian. *J. Chem. Phys.* **1988**, *89*, 7367−7381.
(63) Cederbaum, L. S.; Schirmer, J.; Meyer, H.-D. Block Diagonalisation of Hermitian Matrices. *J. Phys. A* **1989**, *22*, 2427−2439.
(64) Domcke, W.; Woywod, C.; Stengle, M. Diabatic CASSCF Orbitals and Wavefunctions. *Chem. Phys. Lett.* **1994**, *226*, 257−262.
(65) Gadéa, F. X.; Pélissier, M. Approximately Diabatic States: A Relation Between Effective Hamiltonian Techniques and Explicit Cancellation of the Derivative Coupling. *J. Chem. Phys.* **1990**, *93*, 545−551.
(66) des Cloizeaux, J. Extension d'une Formule de Lagrange à des Problèmes de Valeurs Propres. *Nucl. Phys.* **1960**, *20*, 321−346.
(67) Baer, M. Adiabatic and Diabatic Representations for Atom-Molecule Collisions: Treatment of the Collinear Arrangement. *Chem. Phys. Lett.* **1975**, *35*, 112−118.
(68) Top, Z. H.; Baer, M. Incorporation of Electronically Nonadiabatic Effects into Bimolecular Reactive Systems. I. Theory. *J. Chem. Phys.* **1977**, *66*, 1363−1371.
(69) Mead, C. A.; Truhlar, D. G. Conditions for the Definition of a Strictly Diabatic Electronic Basis for Molecular Systems. *J. Chem. Phys.* **1982**, *77*, 6090−6098.
(70) Dederichs, P. H.; Blügel, S.; Zeller, R.; Akai, H. Ground States of Constrained Systems: Application to Cerium Impurities. *Phys. Rev. Lett.* **1984**, *53*, 2512−2515.
(71) Wu, Q.; Van Voorhis, T. Extracting Electron Transfer Coupling Elements from Constrained Density Functional Theory. *J. Chem. Phys.* **2006**, *125*, 164105.
(72) Spiegelmann, F.; Malrieu, J. P. The Use of Effective Hamiltonians for the Treatment of Avoided Crossings. II. Nearly Diabatic Potential Curves. *J. Phys. B* **1984**, *17*, 1259−1279.

(73) Warshel, A.; Weiss, R. M. An Empirical Valence Bond Approach for Comparing Reactions in Solutions and in Enzymes. *J. Am. Chem. Soc.* **1980**, *102*, 6218−6226.
(74) Voth, G. A. Computer Simulation of Proton Solvation and Transport in Aqueous and Biomolecular Systems. *Acc. Chem. Res.* **2006**, *39*, 143−150.
(75) Kamerlin, S. C. L.; Warshel, A. The Empirical Valence Bond Model: Theory and Applications. *WIREs Comput. Mol. Sci.* **2011**, *1*, 30−45.
(76) Wu, W.; Su, P.; Shaik, S.; Hiberty, P. G. Classical Valence Bond Approach by Modern Methods. *Chem. Rev.* **2011**, *111*, 7557−7593.
(77) Mo, Y.; Gao, J. An Ab Initio Molecular Orbital−Valence Bond (MOVB) Method for Simulating Chemical Reactions in Solution. *J. Phys. Chem. A* **2000**, *104*, 3012−3020.
(78) Mo, Y.; Gao, J. Ab Initio QM/MM Simulations with a Molecular Orbital−Valence Bond (MOVB) Method: Application to an S_N2 Reaction in Water. *J. Comput. Chem.* **2000**, *21*, 1458−1469.
(79) Mo, Y.; Peyerimhoff, S. D. Theoretical Analysis of Electronic Delocalization. *J. Chem. Phys.* **1998**, *109*, 1687−1697.
(80) Mo, Y.; Zhang, Y.; Gao, J. A Simple Electronic Model for Trisilylamine: Theoretical Examinations of the n → σ^* Negative Hyperconjugation, $p_\pi \rightarrow d_\pi$ Bonding, and Stereoelectronic Interaction. *J. Am. Chem. Soc.* **1999**, *121*, 5737−5742.
(81) Mo, Y.; Song, L.; Wu, W.; Zhang, Q. Charge Transfer in the Electron Donor−Acceptor Complex BH_3NH_3. *J. Am. Chem. Soc.* **2004**, *126*, 3974−3982.
(82) Chen, Z.; Mo, Y. Electron Transfer in Electrophilic Aromatic Nitration and Nitrosation: Computational Evidence for the Marcus Inverted Region. *J. Chem. Theory Comput.* **2013**, *9*, 4428−4435.
(83) Nakamura, H.; Truhlar, D. G. The Direct Calculation of Diabatic States Based on Configurational Uniformity. *J. Chem. Phys.* **2001**, *115*, 10353−10372.
(84) Nakamura, H.; Truhlar, D. G. Direct Diabatization of Electronic States by the Fourfold Way. II. Dynamical Correlation and Rearrangement Processes. *J. Chem. Phys.* **2002**, *117*, 5576−5593.
(85) Nakamura, H.; Truhlar, D. G. Extension of the Fourfold Way for Calculation of Global Diabatic Potential Energy Surfaces of Complex, Multiarrangement, Non-Born−Oppenheimer Systems: Application to HNCO(S_0, S_1). *J. Chem. Phys.* **2003**, *118*, 6816−6829.
(86) Subotnik, J. E.; Yeganeh, S.; Cave, R. J.; Ratner, M. A. Constructing Diabatic States from Adiabatic States: Extending Generalized Mulliken−Hush to Multiple Charge Centers with Boys Localization. *J. Chem. Phys.* **2008**, *129*, 244101.
(87) Cave, R. J.; Newton, M. D. Generalization of the Mulliken−Hush Treatment for the Calculation of Electron Transfer Matrix Elements. *Chem. Phys. Lett.* **1996**, *249*, 15−19.
(88) Cave, R. J.; Newton, M. D. Calculation of Electronic Coupling Matrix Elements for Ground and Excited State Electron Transfer Reactions: Comparison of the Generalized Mulliken−Hush and Block Diagonalization Methods. *J. Chem. Phys.* **1997**, *106*, 9213−9226.
(89) Migliore, A.; Corni, S.; Di Felice, R.; Molinar, E. First-Principles Density-Functional Theory Calculations of Electron-Transfer Rates in Azurin Dimers. *J. Chem. Phys.* **2006**, *124*, 064501.
(90) Boys, S. F. Construction of Some Molecular Orbitals To Be Approximately Invariant for Changes from One Molecule to Another. *Rev. Mod. Phys.* **1960**, *32*, 296−299.
(91) Olsen, S.; McKenzie, R. H. A Dark Excited State of Fluorescent Protein Chromophores, Considered As Brooker Dyes. *Chem. Phys. Lett.* **2010**, *492*, 150−156.
(92) Olsen, S.; McKenzie, R. H. Bond alternation, polarizability, and resonance detuning in methine dyes. *J. Chem. Phys.* **2011**, *134*, 114520.
(93) Park, J. W.; Rhee, Y. M. Towards the Reliability of Ab Initio Dynamics at the Speed of Molecular Mechanics: Dynamics Simulations of the Green Fluorescent Protein Chromophore with Interpolated Diabatic Hamiltonian. *ChemPhysChem* **2014**, *15*, 3183−3193.
(94) Feng, X.; Luzanov, A. V.; Krylov, A. I. Fission of Entangled Spins: An Electronic Structure Perspective. *J. Phys. Chem. Lett.* **2013**, *4*, 3845−3852.
(95) Szabo, A.; Ostlund, N. S. *Modern Quantum Chemistry: Introduction to Advanced Electronic Structure Theory*; McGraw-Hill: New York, 1989.
(96) Bayly, C. I.; Cieplak, P.; Cornell, W.; Kollman, P. A. A Well-Behaved Electrostatic Potential Based Method Using Charge Restraints for Deriving Atomic Charges: The RESP Model. *J. Phys. Chem.* **1993**, *97*, 10269−10280.
(97) Foresman, J. B.; Head-Gordon, M.; Pople, J. A.; Frisch, M. J. Toward a Systematic Molecular Orbital Theory for Excited States. *J. Phys. Chem.* **1992**, *96*, 135−149.
(98) Head-Gordon, M.; Rico, R. J.; Oumi, M.; Lee, T. J. A Doubles Correction to Electronic Excited States from Configuration Interaction in the Space of Single Substitutions. *Chem. Phys. Lett.* **1994**, *219*, 21−29.
(99) Casanova, D.; Rhee, Y. M.; Head-Gordon, M. Quasidegenerate Scaled Opposite Spin Second Order Perturbation Corrections to Single Excitation Configuration Interaction. *J. Chem. Phys.* **2008**, *128*, 164106.
(100) Rhee, Y. M.; Casanova, D.; Head-Gordon, M. Quartic-Scaling Analytical Gradient of Quasidegenerate Scaled Opposite Spin Second-Order Perturbation Corrections to Single Excitation Configuration Interaction. *J. Chem. Theory Comput.* **2009**, *5*, 1224−1236.
(101) Werner, H.-J. Third-order Multireference Perturbation Theory The CASPT3Method. *Mol. Phys.* **1996**, *89*, 645−661.
(102) Celani, P.; Werner, H.-J. Analytical Energy Gradients for Internally Contracted Second-Order Multireference Perturbation Theory. *J. Chem. Phys.* **2003**, *119*, 5044−5057.
(103) Andersson, K.; Malmqvist, P.-Å.; Roos, B. O. Second-Order Perturbation Theory with a Complete Active Space Self-Consistent Field Reference Function. *J. Chem. Phys.* **1992**, *96*, 1218−1226.
(104) Helgaker, T.; Jørgensen, P.; Olsen, J. *Molecular Electronic-Structure Theory*; John Wiley & Sons: Chichester, 2000.
(105) Nelson, R. B. Simplified Calculation of Eigenvector Derivatives. *AIAA J.* **1976**, *14*, 1201−1205.
(106) Fletcher, R. *Practical Methods of Optimization*; Wiley: New York, 1987.
(107) Berendsen, H. J. C.; Postma, J. P. M.; van Gunsteren, W. F.; DiNola, A.; Haak, J. R. Molecular Dynamics with Coupling to an External Bath. *J. Chem. Phys.* **1984**, *81*, 3684−3690.
(108) Nosé, S. A Unified Formulation of the Constant Temperature Molecular Dynamics Methods. *J. Chem. Phys.* **1984**, *81*, 511−519.
(109) Parrinello, M.; Rahman, A. Polymorphic Transitions in Single Crystals: A New Molecular Dynamics Method. *J. Appl. Phys.* **1981**, *52*, 7182−7190.
(110) Jorgensen, W. L.; Chandrasekhar, J.; Madura, J. D.; Impey, R. W.; Klein, M. L. Comparison of Simple Potential Functions for Simulating Liquid Water. *J. Chem. Phys.* **1983**, *79*, 926−935.
(111) Tully, J. C. Molecular Dynamics with Electronic Transitions. *J. Chem. Phys.* **1990**, *93*, 1061−1071.
(112) Hammes-Schiffer, S.; Tully, J. C. Proton Transfer in Solution: Molecular Dynamics with Quantum Transitions. *J. Chem. Phys.* **1994**, *101*, 4657−4667.
(113) Landau, L. D. Zur Theorie der Energieübertragung bei Stößen II. *Phys. Z. Sowjetunion* **1932**, *2*, 46−51.
(114) Zener, C. Non-Adiabatic Crossing of Energy Levels. *Proc. R. Soc. London A* **1932**, *137*, 696−702.
(115) Fabiano, E.; Keal, T. W.; Thiel, W. Implementation of Surface Hopping Molecular Dynamics Using Semiempirical Methods. *Chem. Phys.* **2008**, *349*, 334−347.
(116) Werner, H.-J.; Knowles, P. J.; Lindh, R.; Manby, F. R.; Schütz, M.; Celani, P.; Korona, T.; Mitrushenkov, A.; Adler, T. B.; Amos, R. D., et al. *MOLPRO: A Package of Ab Initio Programs*, version 2010.1; 2010.
(117) Shao, Y.; Fusti Molnar, L.; Jung, Y.; Kussmann, J.; Ochsenfeld, C.; Brown, S. T.; Gilbert, A. T. B.; Slipchenko, L. V.; Levchenko, S. V.; O'Neill, D. P.; et al. Advances in Methods and Algorithms in a Modern Quantum Chemistry Program Package. *Phys. Chem. Chem. Phys.* **2006**, *8*, 3172−3191.

(118) Glendening, E. D.; Badenhoop, J. K.; Reed, A. E.; Carpenter, J. E.; Bohmann, J. A.; Morales, C. M.; Weinhold, F. *NBO 5.0*; Theoretical Chemistry Institute, University of Wisconsin: Madison, 2001.
(119) Hess, B.; Kutzner, C.; van der Spoel, D.; Lindahl, E. GROMACS 4: Algorithms for Highly Efficient, Load-Balanced, and Scalable Molecular Simulation. *J. Chem. Theory Comput.* **2008**, *4*, 435−447.
(120) Hayashi, S.; Kato, S. Theoretical Study of Intramolecular Long-Range Electron Transfer Reactions between Porphyrin and Benzoquinone: Ab Initio Calculations of Electronic Coupling Element. *J. Phys. Chem. A* **1998**, *102*, 2878−2887.
(121) Frutos, L. M.; Andruniów, T.; Santoro, F.; Ferré, N.; Olivucci, M. Tracking the Excited-state Time Evolution of the Visual Pigment with Multiconfigurational Quantum Chemistry. *Proc. Natl. Acad. Sci. U.S.A.* **2007**, *104*, 7764−7769.
(122) Furse, K. E.; Corcelli, S. A. The Dynamics of Water at DNA Interfaces: Computational Studies of Hoechst 33258 Bound to DNA. *J. Am. Chem. Soc.* **2008**, *130*, 13103−13109.
(123) Furse, K. E.; Corcelli, S. A. Effects of Long-Range Electrostatics on Time-Dependent Stokes Shift Calculations. *J. Chem. Theory Comput.* **2009**, *5*, 1959−1967.
(124) Furse, K. E.; Lindquis, B. A.; Corcelli, S. A. Solvation Dynamics of Hoechst 33258 in Water: An Equilibrium and Nonequilibrium Molecular Dynamics Study. *J. Phys. Chem. B* **2008**, *112*, 3231−3239.
(125) Kumar, P. V.; Maroncelli, M. Polar Solvation Dynamics of Polyatomic Solutes: Simulation Studies in Acetonitrile and Methanol. *J. Chem. Phys.* **1995**, *103*, 3038−3060.
(126) Martins, L. R.; Skaf, M. S. Computer Simulations of the Solvation Dynamics of Coumarin 153 in Dimethylsulfoxide. *Chem. Phys. Lett.* **2002**, *370*, 683−689.
(127) Ingrosso, F.; Ladanyi, B. M.; Mennucci, B.; Elola, M. D.; Tomasi, J. Solvation Dynamics in Acetonitrile: A Study Incorporating Solute Electronic Response and Nuclear Relaxation. *J. Phys. Chem. B* **2005**, *109*, 3553−3564.
(128) Maroncelli, M.; Fleming, G. R. Computer Simulation of the Dynamics of Aqueous Solvation. *J. Chem. Phys.* **1988**, *89*, 5044−5069.
(129) Stratt, R. M.; Maroncelli, M. Nonreactive Dynamics in Solution: The Emerging Molecular View of Solvation Dynamics and Vibrational Relaxation. *J. Phys. Chem.* **1996**, *100*, 12981−12996.
(130) Fleming, G. R.; Cho, M. Chromophore-Solvent Dynamics. *Annu. Rev. Phys. Chem.* **1996**, *47*, 109−134.
(131) Horng, M. L.; Gardecki, J. A.; Papazyan, A.; Maroncelli, M. Subpicosecond Measurement of Polar Solvation Dynamics: Coumarin 153 Revisited. *J. Phys. Chem.* **1995**, *99*, 17311−17337.
(132) Ruthmann, J.; Kovalenko, S. A.; Ernsting, N. P.; Ouw, D. Femtosecond Relaxation of 2-Amino-7-nitrofluorene in Acetonitrile: Observation of the Oscillatory Contribution to the Solvent Response. *J. Chem. Phys.* **1998**, *109*, 5466−5468.
(133) Eom, I.; Joo, T. Polar Solvation Dynamics of Coumarin 153 by Ultrafast Time-resolved Fluorescence. *J. Chem. Phys.* **2009**, *131*, 244507.
(134) de Boeij, W. P.; Pshenichnikov, M. S.; Wiersma, D. A. Ultrafast Solvation Dynamics Explored by Femtosecond Photon Echo Spectroscopies. *Annu. Rev. Phys. Chem.* **1998**, *49*, 99−123.
(135) Lang, B.; Angulo, G.; Vauthey, E. Ultrafast Solvation Dynamics of Coumarin 153 in Imidazolium-Based Ionic Liquids. *J. Phys. Chem. A* **2006**, *110*, 7028−7034.
(136) Abbyad, P.; Childs, W.; Shi, X.; Boxer, S. G. Dynamic Stokes Shift in Green Fluorescent Protein Variants. *Proc. Natl. Acad. Sci. U.S.A.* **2007**, *104*, 20189−20194.
(137) Rubtsov, I. V.; Yoshihara, K. Vibrational Coherence in Electron Donor−Acceptor Complexes. *J. Phys. Chem. A* **1999**, *103*, 10202−10212.